LETTER

doi:10.1038/nature25975

Human hippocampal neurogenesis drops sharply in children to undetectable levels in adults

Shawn F. Sorrells[1,2]*, Mercedes F. Paredes[1,3]*, Arantxa Cebrian-Silla[4], Kadellyn Sandoval[1,3], Dashi Qi[5], Kevin W. Kelley[1], David James[1], Simone Mayer[1,3], Julia Chang[6], Kurtis I. Auguste[2], Edward F. Chang[2], Antonio J. Gutierrez[7], Arnold R. Kriegstein[1,3], Gary W. Mathern[8,9], Michael C. Oldham[1,2], Eric J. Huang[10], Jose Manuel Garcia-Verdugo[4], Zhengang Yang[5] & Arturo Alvarez-Buylla[1,2]

New neurons continue to be generated in the subgranular zone of the dentate gyrus of the adult mammalian hippocampus[1–5]. This process has been linked to learning and memory, stress and exercise, and is thought to be altered in neurological disease[6–10]. In humans, some studies have suggested that hundreds of new neurons are added to the adult dentate gyrus every day[11], whereas other studies find many fewer putative new neurons[12–14]. Despite these discrepancies, it is generally believed that the adult human hippocampus continues to generate new neurons. Here we show that a defined population of progenitor cells does not coalesce in the subgranular zone during human fetal or postnatal development. We also find that the number of proliferating progenitors and young neurons in the dentate gyrus declines sharply during the first year of life and only a few isolated young neurons are observed by 7 and 13 years of age. In adult patients with epilepsy and healthy adults (18–77 years; $n = 17$ post-mortem samples from controls; $n = 12$ surgical resection samples from patients with epilepsy), young neurons were not detected in the dentate gyrus. In the monkey (*Macaca mulatta*) hippocampus, proliferation of neurons in the subgranular zone was found in early postnatal life, but this diminished during juvenile development as neurogenesis decreased. We conclude that recruitment of young neurons to the primate hippocampus decreases rapidly during the first years of life, and that neurogenesis in the dentate gyrus does not continue, or is extremely rare, in adult humans. The early decline in hippocampal neurogenesis raises questions about how the function of the dentate gyrus differs between humans and other species in which adult hippocampal neurogenesis is preserved.

We used 59 post-mortem and post-operative samples of the human hippocampus (Supplementary Table 1) to investigate the presence of progenitor cells and young neurons from fetal to adulthood stages. At 14 gestational weeks, at the peak of proliferation in the fetal dentate gyrus (DG)[15], many dividing (Ki-67$^+$) neural progenitors (SOX1$^+$ (ref. 16) and SOX2$^+$ (ref. 17)) were observed in the dentate neuroepithelium (dNE; Fig. 1a, Extended Data Fig. 1a–c and Supplementary Video 1). A continuous region of Ki-67$^+$SOX1$^+$ and Ki-67$^+$SOX2$^+$ cells, associated with ribbons of nestin$^+$vimentin$^+$ fibres and cells, was observed between the dNE and the proximal blade of the DG. At 22 gestational weeks, the proliferating cells between the dNE and the DG were greatly diminished, and most Ki-67$^+$SOX1$^+$ or Ki-67$^+$SOX2$^+$ cells in the hippocampus were found in the hilus (Fig. 1b and Extended Data Fig. 1d–f). By this age, most young neurons (DCX$^+$PSA-NCAM$^+$ cells), were concentrated in the granule cell layer (GCL) proximal to the dNE (Fig. 1c). By contrast, the distal GCL contained higher numbers of mature NeuN$^+$ neurons (Extended Data Fig. 1g, h), suggesting a gradient of maturation.

To look for the formation of a proliferative subgranular zone (SGZ), we characterized dividing and progenitor cells in the human DG from fetal development to adulthood. At 22 gestational weeks, Ki-67$^+$ cells were predominantly observed in the hilus and next to the distal GCL (Figs 1b, 2a). By early postnatal life, Ki-67$^+$ cells remained distributed throughout the hilus and GCL (Fig. 2a). The number of Ki-67$^+$Sox1$^+$ or Ki-67$^+$Sox2$^+$ cells decreased in the hilus during the first year of life (Fig. 2b–d), but these cells did not form a discrete layer beneath the GCL at any of the ages studied (Fig. 2a–d). There were rare instances of SOX2$^+$Ki-67$^+$ cells in the DG of a 35-year-old individual, but these cells were BLBP$^-$ and were dispersed throughout the hippocampus. Light and electron microscopy images of samples obtained from individuals at 22 gestational weeks, birth and 7, 18 and 48 years of age did not reveal a layer of cells with progenitor characteristics adjacent to the GCL (Extended Data Figs 2a–c, 3). Ki-67$^+$BLBP$^+$ cells were found in the developing DG during fetal and early postnatal stages, but BLBP$^+$ cells were Ki-67$^-$ in juvenile and adult brains and were located primarily in the molecular layer (Extended Data Figs 1a, 2b). Furthermore, immunostaining for nestin, vimentin or GFAP in brain sections from individuals that were 7 years of age and older did not show cells next to the DG or in the hilus that had the typical neural progenitor/stem cell morphology of radial astrocytes (also known as radial or type-I cells)[3,4,18]. BLBP and vimentin were depleted from the hilus and were predominantly expressed in mature stellar astrocytes in the molecular layer in brains from individuals that were 7 years of age and older. GFAP-expressing cells that remained in the adult hilus were stellate ALDH1L1$^+$ astrocytes with thin fibres that extended through the hilus and GCL (Extended Data Figs 3a, d, 4). These cells were not Ki-67$^+$ or found in mitosis. These results indicate that a germinal SGZ does not form next to the human GCL, and that proliferating cells, which express progenitor/stem cell markers, are mostly depleted from the hilus by 7 years of age.

We next investigated the presence of young neurons in the postnatal, human DG. At birth, DCX$^+$PSA-NCAM$^+$ cells were located across the GCL, frequently in clusters (Fig. 3a, b). The number of DCX$^+$PSA-NCAM$^+$ cells in the GCL decreased from $1{,}618 \pm 780$ (mean $\pm$ s.d.) cells per mm^2 at birth to 292.9 ± 142.8 cells per mm^2 at 1 year of age. By 7 years of age, 12.4 ± 5.3 DCX$^+$PSA-NCAM$^+$ cells per mm^2 were found in the GCL and at 13 years of age, the GCL contained

[1]Eli and Edythe Broad Center of Regeneration Medicine and Stem Cell Research, University of California San Francisco, San Francisco, California 94143, USA. [2]Department of Neurological Surgery, University of California San Francisco, San Francisco, California 94143, USA. [3]Department of Neurology, University of California San Francisco, San Francisco, California 94143, USA. [4]Laboratorio de Neurobiología Comparada, Instituto Cavanilles, Universidad de Valencia, CIBERNED, Valencia, 46980, Spain. [5]State Key Laboratory of Medical Neurobiology and Institutes of Brain Science, Department of Neurology, Zhongshan Hospital, Fudan University, Shanghai, 200032, China. [6]David Geffen School of Medicine, Department of Neurosurgery, Intellectual Development and Disabilities Research Center, University of California Los Angeles, Los Angeles, California 90095, USA. [7]Unidad de Cirugía de la Epilepsia, Hospital Universitario La Fe, Valencia 46026, Spain. [8]Department of Neurosurgery, David Geffen School of Medicine, University of California Los Angeles, Los Angeles, California 90095, USA. [9]Department of Psychiatry and Biobehavioral Medicine, David Geffen School of Medicine, University of California Los Angeles, Los Angeles, California 90095, USA. [10]Department of Pathology, University of California San Francisco, San Francisco, California 94143, USA.

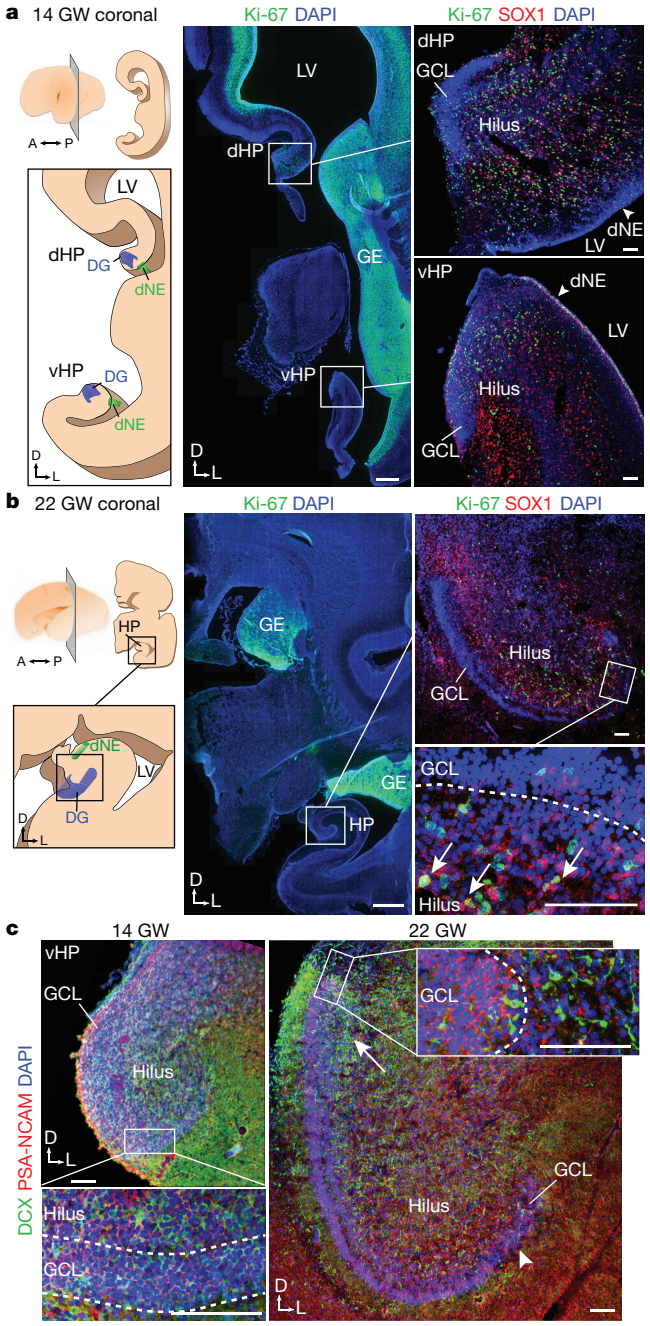

Figure 1 | Early fetal development of the human DG. a, Left, schematic of one hemisphere at 14 gestational weeks (GW), coronal section showing the lateral ventricle (LV) and ganglionic eminence (GE). Middle and right, immunofluorescence images. Ki-67$^+$SOX1$^+$ cells were found in the dorsal (dHP) and ventral (vHP) hippocampus. A, anterior; D, dorsal, L, lateral; P, posterior. **b**, Left, schematic of one hemisphere at 22 gestational weeks, coronal section. Middle and right, SOX1$^+$Ki-67$^+$ cells in the hilus and GCL (arrows). **c**, Distribution of DCX$^+$PSA-NCAM$^+$ cells at 14 gestational weeks and 22 gestational weeks. The arrow indicates the end of the GCL most proximal to the dNE. The distal end of the GCL contained fewer young neurons (arrowhead). Scale bars, 1 mm (**a**, **b** (middle)) and 100 μm (**a**, **b** (right), **c**). Staining was replicated at least three times ($n = 1$ at 14 gestational weeks; $n = 3$ at 22 gestational weeks).

2.4 ± 0.74 DCX$^+$PSA-NCAM$^+$ cells per mm^2 (that is, approximately 1–2 DCX$^+$PSA-NCAM$^+$ cells per section; Fig. 3c–e and Extended Data Fig. 5). DCX$^+$ cells in the DG of infants (1 year old or less) not only expressed PSA-NCAM, but also frequently had the simple elongated morphology of young neurons (Extended Data Fig. 5b). By contrast, light and electron microscopy images of sections from the brain of a 7-year-old individual showed that the DG contained DCX$^+$ cells in different stages of maturation (Extended Data Fig. 6a). DCX$^+$ cells in the hippocampus of a 13-year-old individual had a more mature morphology (Fig. 3e), expressed NeuN and had distinct axons and dendrites (Extended Data Fig. 5c). We examined hippocampuses of 17 individuals that were between 18 and 77 years old when they died (Supplementary Table 1) for evidence of young neurons. In two adults (sample numbers 24 and 26), we also studied the ventricular wall and found rare DCX$^+$ cells with a migratory morphology in the ventricular–subventricular zone[19,20], providing a positive control (Extended Data Fig. 6b). We found no evidence of DCX$^+$PSA-NCAM$^+$ young neurons in the hilus or GCL of the hippocampuses from these individuals (Extended Data Figs 5d, 6b). At three weeks of age, there were many DCX$^+$TUJ1$^+$ young neurons in the GCL, however, we did not detect these cells at 19 or 36 years of age. In adults, we observed TUJ1$^+$ fibres that belonged to many mature neurons (Extended Data Fig. 6c). PSA-NCAM$^+$ cells were present in the hilus and GCL of adult brains, but these cells had a mature neuronal morphology and were NeuN$^+$ (Extended Data Fig. 5d–f). Using single-molecule *in situ* hybridization labelling of *DCX* transcripts, we detected many DCX$^+$ cells in the GCL at 14 gestational weeks, but only weak signal in very few, widely distributed cells at 13 years (Extended Data Fig. 6d). A subpopulation of cells with round nuclei was occasionally labelled by DCX antibodies. These DCX$^+$ cells had multiple processes, were not restricted to the hippocampus, expressed the glial markers IBA1 or OLIG2, and had ultrastructural features of glia (Extended Data Fig. 7).

We also analysed the proliferation of progenitor cells and the presence of young neurons in surgical resections of patients with epilepsy that contained the hippocampus (Supplementary Table 1). In these samples, Ki-67$^+$BLBP$^+$SOX2$^+$ or Ki-67$^+$SOX1$^+$vimentin$^+$ cells were present in the hilus and GCL of a 10-month-old individual, but were absent from the sample of an 11-year-old individual (Extended Data Fig. 8a, b). We also found many DCX$^+$PSA-NCAM$^+$ cells at 10 months, whereas only a few cells per section were found in samples from a 7-year-old individual and none were found in 13 surgical resections from individuals that were older than 11 years of age (Extended Data Fig. 8c–g). There was no evidence of a discrete layer of dividing cells or young neurons in any of the adult cases with epilepsy that we studied.

We next searched for proliferative progenitors and young neurons in the rhesus macaque (*M. mulatta*). Early studies[2], in which thymidine-labelling was used, found no evidence of newly generated neurons in adult macaques (17 years old), but subsequent work[21] using injections of 5-bromodeoxyuridine (BrdU, a thymidine analogue that labels newly generated cells) were used, have suggested that low levels of neurogenesis occur, even in the DG of 23-year-old monkeys. At embryonic day (E)150, we observed remnants of the migratory stream between the dNE and the proximal blade of the developing DG (Extended Data Fig. 9a). Ki-67$^+$ and DCX$^+$ cells consolidated into a layer in the SGZ between E150 and birth (Fig. 4 and Extended Data Fig. 9a–c). Between birth and 1.5 years of age, the number of Ki-67$^+$ cells decreased eightfold and the macaque SGZ became less defined (Fig. 4a). The average number of proliferating cells decreased 35-fold between 1.5 and 7 years of age (Fig. 4e). A continuous SGZ was not detected in macaques that were older than 7 years. Instead, isolated, small, dark cells and occasional Ki-67$^+$ cells were observed next to the GCL (Fig. 4a and Extended Data Fig. 9b). Similarly, the number of DCX$^+$PSA-NCAM$^+$ young neurons decreased during this period, becoming sparse and discontinuous by 7 years of age (Fig. 4b–d, f). Most DCX$^+$PSA-NCAM$^+$ cells in samples from macaques that were 5 years and older had round nuclei and extensive dendritic trees (Fig. 4c, d and Extended Data Fig. 9d), but some retained the elongated morphology and ultrastructure of young neurons (Fig. 4d, g). Although DCX$^+$ cells in the DG of 22- and 23-year-old macaques were rare, they were readily found in the ventricular–subventricular zone and rostral migratory stream[22] (Extended Data Fig. 9e). We next used BrdU to

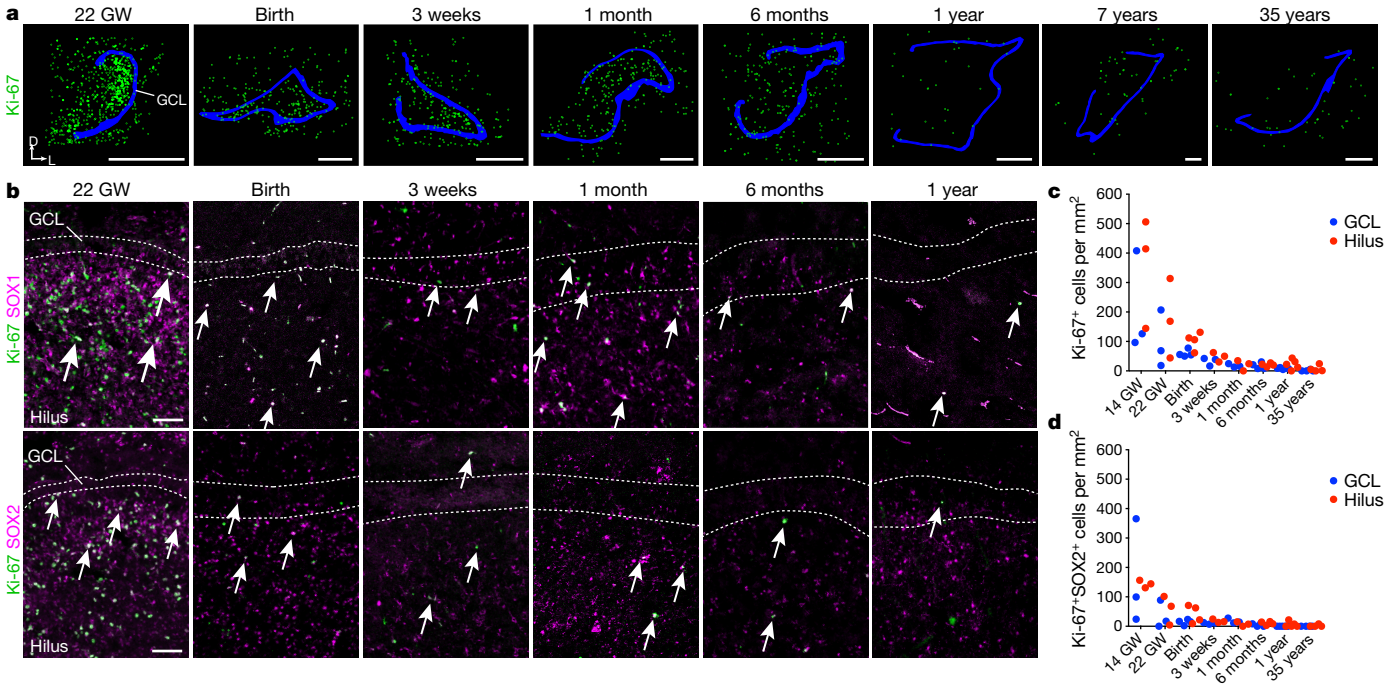

Figure 2 | Human DG proliferation declines sharply during infancy and a layer of proliferating progenitors does not form in the SGZ. **a**, Maps of Ki-67$^+$ (green) cells in the DG from samples of individuals that were between 22 gestational weeks and 35 years of age; GCL in blue. **b**, Ki-67$^+$SOX1$^+$ and Ki-67$^+$SOX2$^+$ cells (arrows) are distributed across the hilus and GCL and the number of double-positive cells decreases between 22 gestational weeks and 1 year of age. **c**, **d**, Quantification of Ki-67$^+$ (**c**) and Ki-67$^+$SOX2$^+$ (**d**) cells in the hilus and GCL. For quantifications, dots indicate staining replicates ($\geq$3) (each age $n = 1$). Scale bars, 1 mm (**a**) and 100 μm (**b**).

label recently dividing cells in two 1.5-year-old macaques; at this age the SGZ contained markers of progenitors and young neurons (Extended Data Fig. 9f, g). We checked for BrdU staining 10 and 15 weeks after five days of twice-daily BrdU (50 mg kg^{-1}) injections. DCX$^+$BrdU$^+$ and a few NeuN$^+$BrdU$^+$ cells were observed in the SGZ and GCL (Extended Data Fig. 9h, i and Supplementary Table 4). By contrast, in the brains of 7-year-old macaques that received the same BrdU treatment, we found no DCX$^+$BrdU$^+$ cells in the SGZ 10 weeks after BrdU

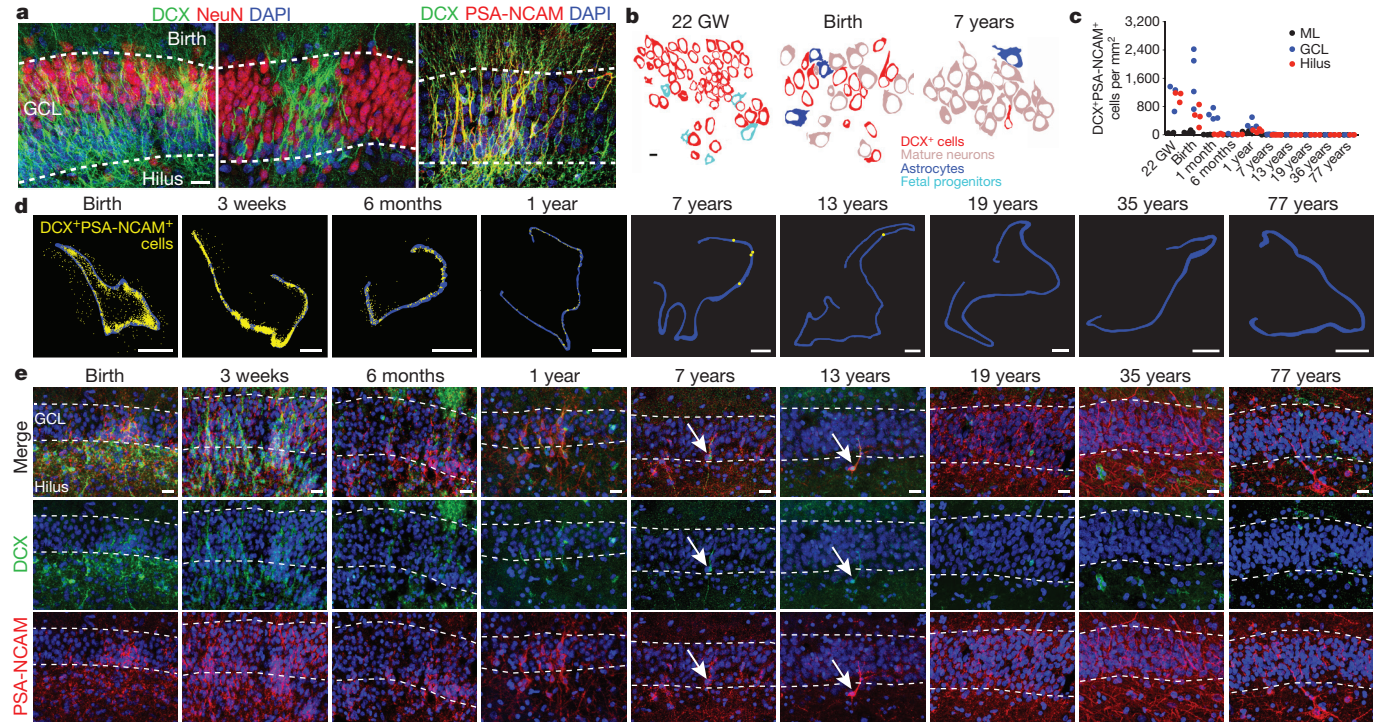

Figure 3 | The number of young neurons declines in the human DG from infancy into childhood. **a**, DCX$^+$ cells at birth are distributed in a continuous field (left) or tight clusters (middle) and express PSA-NCAM (right). **b**, Outlines of cell types in the GCL at 22 gestational weeks, birth and 7 years of age. **c**, Quantification of DCX$^+$PSA-NCAM$^+$ cells in the DG. **d**, Maps of DCX$^+$PSA-NCAM$^+$ cells (yellow dots; GCL, blue outline). **e**, DCX$^+$PSA-NCAM$^+$ cells in the DG (birth to 77 years) are rare by 7 and 13 years of age (arrows). For quantifications, dots indicate staining replicates ($\geq$3) (each age, $n = 1$). Scale bars, 1 mm (**d**), 20 μm (**a**, **e**) and 5 μm (**b**).

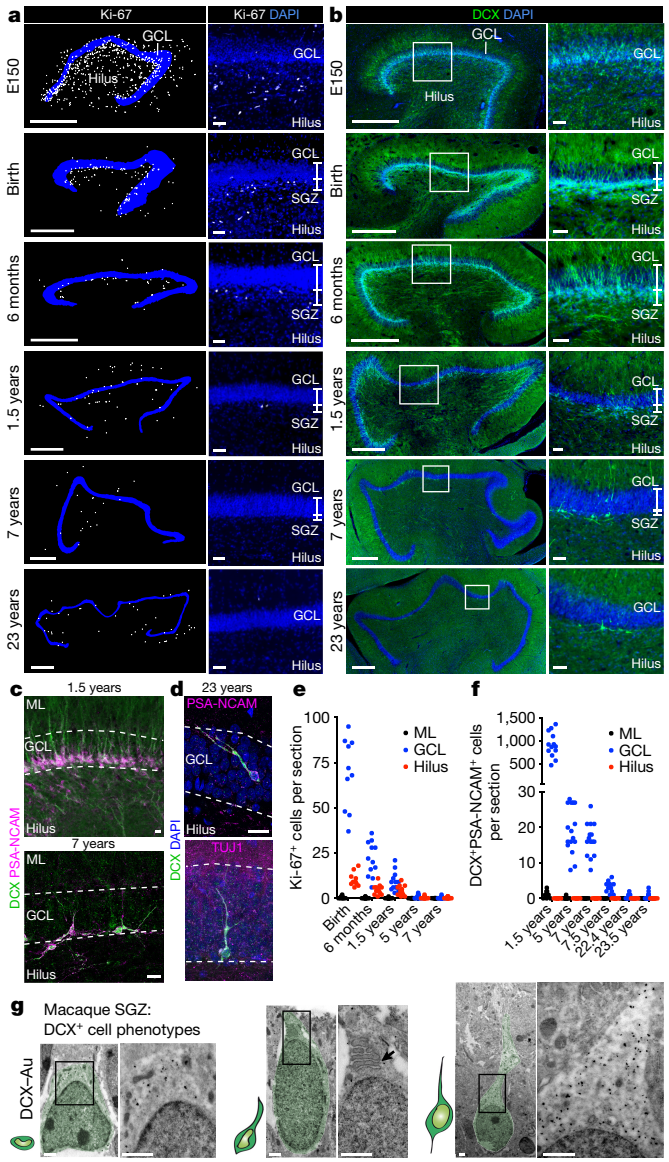

Figure 4 | The SGZ forms during macaque development but new neurons are rare in adults. a, **b**, Maps and immunostaining of Ki-67$^+$ cells (**a**) and DCX$^+$ cells (**b**) in the macaque SGZ (from E150 to 23 years of age). **c**, DCX$^+$PSA-NCAM$^+$ cells in the SGZ (1.5 and 7 years). **d**, DCX$^+$PSA-NCAM$^+$ or DCX$^+$TUJ1$^+$ cells (23 years). **e**, **f**, Quantification of Ki-67$^+$ cells (**e**) and DCX$^+$PSA-NCAM$^+$ cells (**f**) in the macaque GCL, hilus and molecular layer (ML). $n = 1$ animal per age; dots indicate staining replicates (≥ 3). **g**, Immunogold (DCX–Au) transmission electron microscopy of neurons (light green overlay) at different stages of maturation. Left, small DCX$^+$ cell; middle, DCX$^+$ cell with a short process, mitochondria and prominent endoplasmic reticulum (arrow); right, large DCX$^+$ cell with round soma, few organelles and an expansion into the GCL. Scale bars, 500 μm (**a**, **b** (left)), 50 μm (**a**, **b** (right)), 20 μm (**c**, **d**) and 1 μm (**g**).

treatment; 15 weeks after BrdU treatment, we found two DCX$^+$BrdU$^+$ cells (Extended Data Fig. 9j and Supplementary Table 4). We did not find NeuN$^+$BrdU$^+$ cells in the GCL of these 7-year-old monkeys. Given the higher level of neurogenesis observed in the 1.5-year-old macaque, we studied one monkey at this age 2 h after a single BrdU injection. Many BrdU$^+$ cells that expressed the proliferative markers, Ki-67 and MCM2, and the progenitor marker, SOX2, were present in the SGZ (Extended Data Fig. 9h). Finally, we compared hippocampal gene expression profiles from macaque and human (Extended Data Fig. 10). A sharp decrease in DCX, TUJ1 and Ki-67 expression was observed in both species. In normalized developmental time, the decrease in DCX-expressing cells was accelerated in human compared to macaque (Extended Data Fig. 10). We conclude that there is a marked decrease in neurogenesis in the macaque DG during juvenile development, and that rare DCX$^+$PSA-NCAM$^+$ young neurons occur in adults.

In the rodent brain, a proliferative SGZ consolidates around postnatal day (P)10[23,24], and neural stem cells within this region continue to generate new neurons into adulthood[4]. In the human brain, however, we did not find an equivalent proliferative region at any of the ages analysed. Ki-67$^+$ cells were distributed throughout the fetal and infant hilus and GCL. The adult human SGZ was devoid of precursor cells and young neurons, and instead contained many ALDH1L1$^+$GFAP$^+$ cells. It is intriguing that we found rare examples of SOX2$^+$Ki-67$^+$ cells in the adult DG, but these cells were not confined to the hilus or GCL and were BLBP$^-$. We cannot exclude the possibility that neural stem cells in humans are BLBP$^-$ or are highly dispersed, but we did not observe DCX$^+$PSA-NCAM$^+$ cells in these samples. The simplest explanation is that these cells are dividing local glia, many of which are known to express SOX2[25,26] (Extended Data Fig. 3c). The lack of a coalesced SGZ could explain the absence (or rarity) of DG neurogenesis in the adult human brain.

The above findings do not support the notion that robust adult neurogenesis continues in the human hippocampus (see Supplementary Discussion). ^{14}C dating on sorted NeuN$^+$ nuclei[11] has suggested that many new neurons continue to be generated in the adult human hippocampus, with little decline with age, but additional evidence for high levels of progenitors or young neurons was not shown. Interestingly, considerable interindividual variation was observed in this study, and many individual samples had ^{14}C levels consistent with no, or little, postnatal neuronal addition. Labelled neuronal cells in the GCL in patients that received a low dose of BrdU[13], could possibly be explained by processes not associated with cell division[27,28] (Extended Data Fig. 7f). Other groups find a sharp decline with age in proliferation and markers of DG neurogenesis[12,14,29], consistent with the above findings. It has been suggested that a few new neurons continue to be produced in adults based on DCX expression detected by PCR or western blot[14,29,30]. However, glial cells can express DCX[26] (Extended Data Fig. 7c–e), possibly explaining some of these expression data. The lack of young neurons in our adult human DG samples could be due to processes linked to disease and/or death. However, similar results were obtained in DG from intraoperative samples or from patients with diverse causes of death. By contrast, young neurons were found in epilepsy samples from children and in our control paediatric cases, despite diverse clinical histories. In contrast to our observations in humans, we observed a germinal SGZ in the young macaques. We found that neurogenesis continues postnatally in macaques, but like humans, this process declined in juveniles and adults, consistent with previous ^{3}H-thymidine and BrdU studies[2,21,31]. If neurogenesis continues in the adult human hippocampus, this is a rare phenomenon, raising questions of how human DG plasticity differs from other species in which adult hippocampal neurogenesis is abundant. Interestingly, a lack of neurogenesis in the hippocampus has been suggested for aquatic mammals (dolphins, porpoises and whales)[5], species known for their large brains, longevity and complex behaviour. Understanding the limitations of adult neurogenesis in humans and other species is fundamental to interpreting findings from animal models.

Online Content Methods, along with any additional Extended Data display items and Source Data, are available in the online version of the paper; references unique to these sections appear only in the online paper.

Received 6 April 2017; accepted 6 February 2018.
Published online 7 March 2018.

1. Altman, J. & Das, G. D. Autoradiographic and histological evidence of postnatal hippocampal neurogenesis in rats. *J. Comp. Neurol.* **124,** 319–335 (1965).
2. Kornack, D. R. & Rakic, P. Continuation of neurogenesis in the hippocampus of the adult macaque monkey. *Proc. Natl Acad. Sci. USA* **96,** 5768–5773 (1999).

3. Seri, B., García-Verdugo, J. M., McEwen, B. S. & Alvarez-Buylla, A. Astrocytes give rise to new neurons in the adult mammalian hippocampus. *J. Neurosci.* **21,** 7153–7160 (2001).
4. van Praag, H. *et al.* Functional neurogenesis in the adult hippocampus. *Nature* **415,** 1030–1034 (2002).
5. Patzke, N. *et al.* In contrast to many other mammals, cetaceans have relatively small hippocampi that appear to lack adult neurogenesis. *Brain Struct. Funct.* **220,** 361–383 (2015).
6. Kempermann, G., Kuhn, H. G. & Gage, F. H. More hippocampal neurons in adult mice living in an enriched environment. *Nature* **386,** 493–495 (1997).
7. van Praag, H., Kempermann, G. & Gage, F. H. Running increases cell proliferation and neurogenesis in the adult mouse dentate gyrus. *Nat. Neurosci.* **2,** 266–270 (1999).
8. Lugert, S. *et al.* Quiescent and active hippocampal neural stem cells with distinct morphologies respond selectively to physiological and pathological stimuli and aging. *Cell Stem Cell* **6,** 445–456 (2010).
9. Malberg, J. E. & Duman, R. S. Cell proliferation in adult hippocampus is decreased by inescapable stress: reversal by fluoxetine treatment. *Neuropsychopharmacology* **28,** 1562–1571 (2003).
10. Hill, A. S., Sahay, A. & Hen, R. Increasing adult hippocampal neurogenesis is sufficient to reduce anxiety and depression-like behaviors. *Neuropsychopharmacology* **40,** 2368–2378 (2015).
11. Spalding, K. L. *et al.* Dynamics of hippocampal neurogenesis in adult humans. *Cell* **153,** 1219–1227 (2013).
12. Dennis, C. V., Suh, L. S., Rodriguez, M. L., Kril, J. J. & Sutherland, G. T. Human adult neurogenesis across the ages: an immunohistochemical study. *Neuropathol. Appl. Neurobiol.* **42,** 621–638 (2016).
13. Eriksson, P. S. *et al.* Neurogenesis in the adult human hippocampus. *Nat. Med.* **4,** 1313–1317 (1998).
14. Knoth, R. *et al.* Murine features of neurogenesis in the human hippocampus across the lifespan from 0 to 100 years. *PLoS ONE* **5,** e8809 (2010).
15. Yang, P. *et al.* Developmental profile of neurogenesis in prenatal human hippocampus: an immunohistochemical study. *Int. J. Dev. Neurosci.* **38,** 1–9 (2014).
16. Venere, M. *et al.* Sox1 marks an activated neural stem/progenitor cell in the hippocampus. *Development* **139,** 3938–3949 (2012).
17. Suh, H. *et al. In vivo* fate analysis reveals the multipotent and self-renewal capacities of $Sox2^{+}$ neural stem cells in the adult hippocampus. *Cell Stem Cell* **1,** 515–528 (2007).
18. Steiner, B. *et al.* Type-2 cells as link between glial and neuronal lineage in adult hippocampal neurogenesis. *Glia* **54,** 805–814 (2006).
19. Sanai, N. *et al.* Corridors of migrating neurons in the human brain and their decline during infancy. *Nature* **478,** 382–386 (2011).
20. Wang, C. *et al.* Identification and characterization of neuroblasts in the subventricular zone and rostral migratory stream of the adult human brain. *Cell Res.* **21,** 1534–1550 (2011).
21. Gould, E. *et al.* Hippocampal neurogenesis in adult Old World primates. *Proc. Natl Acad. Sci. USA* **96,** 5263–5267 (1999).
22. Kornack, D. R. & Rakic, P. The generation, migration, and differentiation of olfactory neurons in the adult primate brain. *Proc. Natl Acad. Sci. USA* **98,** 4752–4757 (2001).
23. Sugiyama, T., Osumi, N. & Katsuyama, Y. The germinal matrices in the developing dentate gyrus are composed of neuronal progenitors at distinct differentiation stages. *Dev. Dyn.* **242,** 1442–1453 (2013).
24. Altman, J. & Bayer, S. A. Mosaic organization of the hippocampal neuroepithelium and the multiple germinal sources of dentate granule cells. *J. Comp. Neurol.* **301,** 325–342 (1990).
25. Komitova, M. & Eriksson, P. S. Sox-2 is expressed by neural progenitors and astroglia in the adult rat brain. *Neurosci. Lett.* **369,** 24–27 (2004).
26. Zhang, Y. *et al.* An RNA-sequencing transcriptome and splicing database of glia, neurons, and vascular cells of the cerebral cortex. *J. Neurosci.* **34,** 11929–11947 (2014).
27. Breunig, J. J., Arellano, J. I., Macklis, J. D. & Rakic, P. Everything that glitters isn't gold: a critical review of postnatal neural precursor analyses. *Cell Stem Cell* **1,** 612–627 (2007).
28. Gould, E. How widespread is adult neurogenesis in mammals? *Nat. Rev. Neurosci.* **8,** 481–488 (2007).
29. Mathews, K. J. *et al.* Evidence for reduced neurogenesis in the aging human hippocampus despite stable stem cell markers. *Aging Cell* **16,** 1195–1199 (2017).
30. Fahrner, A. *et al.* Granule cell dispersion is not accompanied by enhanced neurogenesis in temporal lobe epilepsy patients. *Exp. Neurol.* **203,** 320–332 (2007).
31. Eckenhoff, M. F. & Rakic, P. Nature and fate of proliferative cells in the hippocampal dentate gyrus during the life span of the rhesus monkey. *J. Neurosci.* **8,** 2729–2747 (1988).

Supplementary Information is available in the online version of the paper.

Acknowledgements We thank the families who donated the tissue samples used in this study, and J. Rodriguez, V. Tang, J. Cotter and C. Guinto for technical support. S.F.S. was supported by F32 MH103003 and M.F.P. was supported by K08 NS091537. A.A.-B. was supported by NIH grants P01 NS083513, R01 NS028478 and a gift from the John G. Bowes Research Fund. He is the Heather and Melanie Muss Endowed Chair and Professor of Neurological Surgery at UCSF and is a co-founder and serves on the scientific advisory board of Neurona Therapeutics. G.W.M. was partly supported by the Davies/Crandall Endowed Chair For Epilepsy Research at UCLA. G.W.M. and J.C. were supported by NIH NINDS (NS083823 and U01 MH108898). M.C.O. was supported by a Scholar Award from the UCSF Weill Institute for Neurosciences. We acknowledge NSFC grants to Z.Y. (31425011, 31630032, and 31421091). S.M. was supported by fellowships from the European Molecular Biology Organization (EMBO Long-Term Fellowship, ALTF_393-2015) and the German Research Foundation (DFG, MA 7374/1-1). J.M.G.-V. and A.C.-S. were supported by MINECO/FEDER Grant BFU2015-64207-P, Red de Terapia Celular TerCel, Instituto de Salud Carlos III (ISCIII2012-RED-19-016 and RD12/0019/0028) and PROMETEOII/2014/075.

Author Contributions M.F.P. and S.F.S. contributed equally as co-first authors and A.C.-S., K.S. and D.Q. contributed equally as second authors. Z.Y., A.A.-B., M.F.P. and S.F.S. conceived the study. A.A.-B., S.F.S. and M.F.P. designed and interpreted the experiments and, with A.C.-S., K.S., D.Q., S.M. and D.J., conducted the experiments. K.I.A., E.F.C., J.C., E.J.H., A.J.G., A.R.K. and G.W.M. assisted with specimen collection and conducted clinical and neuropathological reviews. K.W.K. and M.C.O. designed and performed the bioinformatic analyses. A.C.-S. and J.M.G.-V. conducted and interpreted the ultrastructural studies. S.F.S., M.F.P., A.C.-S. and K.S. prepared the figures. A.A.-B., S.F.S. and M.F.P. wrote the manuscript with input from all authors.

Author Information Reprints and permissions information is available at www.nature.com/reprints. The authors declare no competing financial interests. Readers are welcome to comment on the online version of the paper. Publisher's note: Springer Nature remains neutral with regard to jurisdictional claims in published maps and institutional affiliations. Correspondence and requests for materials should be addressed to A.A.-B. (AlvarezBuyllaA@ucsf.edu), Z.Y. (yangz@fudan.edu.cn) or J.G.-V. (j.manuel.garcia@uv.es).

METHODS

Human tissue collection. Thirty-seven post-mortem specimens from controls and twenty-two post-operative neurosurgical specimens from patients with epilepsy were collected for this study (Supplementary Table 1). Tissue was collected at the following institutions with previous patient consent in strict observance of the legal and institutional ethical regulations of each participating institution: (1) The University of California, San Francisco (UCSF) Committee on Human Research. Protocols were approved by the Human Gamete, Embryo and Stem Cell Research Committee (Institutional Review Board) at UCSF. (2) The Ethical Committee for Biomedical Investigation, Hospital La Fe (2015/0447) and the University of Valencia Ethical Commission for Human Investigation. (3) In accordance with institutional guidelines and study design approval by the Institutional Review Board (Ethics Committee) of Shanghai Medical College (20110307-085, 20120302-099). (4) Specimens collected at UCLA had Institutional Review Board-approved informed consents for research along with HIPAA authorizations signed by parents or responsible guardians, as per the UCLA Human Research Protection Program. For infant cases, when the brain was at full term (37–40 gestational weeks) and autopsy was performed within two days after birth, we refer to the case as 'birth'. We collected tissue blocks from the temporal lobe, posteriorly from the amygdaloid complex to the posterior end of the inferior horn of the lateral ventricle. Autopsy samples had a post-mortem interval of less than 48 h, and samples from patients with epilepsy had less than 1 h to fixation (in 4% paraformaldehyde (PFA) or 10% formalin). For two adult brains (35-years old and 39-years old), the individuals were perfused within 3–5 h of death with 4% PFA during autopsy via the carotid artery and placed in fixative. All brains were typically cut into approximately 1.5-cm blocks, fixed in 4% PFA for an additional two days, cryoprotected in a 30% sucrose solution, and then frozen in embedding medium (OCT). Blocks were cut into 30-μm sections on a cryostat and mounted on glass slides for immunohistochemistry. For each case, we cresyl-stained a minimum of three sections at different levels to confirm anatomical landmarks and orientation of the sample. Neurosurgical excisions of the temporal lobe, which included the hippocampus, were performed as part of resection treatment in patients with intractable epilepsy as previously described[32]. We recorded the anatomical origin of each intra-operative specimen with intra-operative neuronavigation. Intra-operative specimen assessments were independently confirmed by a neuropathologist. We performed immunohistochemistry staining on surgical sections to look for the expression of PROX1 to confirm the location of the GCL.

Macaque tissue preparation. All animal care and experiments were conducted in accordance with the Fudan University Shanghai Medical College and UC Davis guidelines. Embryonic, neonatal, juvenile and adult macaque monkeys, *M. mulatta*, of both sexes at various ages (Supplementary Table 2), were obtained from the Kunming Primate Research Center of the Chinese Academy of Sciences (Kunming, China), Suzhou Xishan Zhongke Laboratory Animal Co., Ltd (Suzhou, China) and the UC Davis Primate Research Center (Davis, USA). For immunohistochemical staining, postnatal monkeys were deeply anaesthetized and then perfused with PBS followed by 4% PFA. The brains were removed and post-fixed with 4% PFA for 12–48 h. Postnatal brains were then cut coronally into approximately 1.0–2.0-cm slabs and cryoprotected in 30% sucrose in 0.1 M phosphate buffer at 4 °C for 72 h. The brain tissue samples were frozen in embedding medium (OCT) on a dry ice and ethanol slush.

BrdU administration. We used five monkeys to do BrdU labelling experiments: three 1.5-year-old monkeys and two 7–7.5-year-old monkeys. BrdU acute labelling: one 1.5-year-old monkey was injected once intravenously with BrdU (50 mg kg^{-1}) and euthanized 2 h after BrdU injection. BrdU birth dating: BrdU (50 mg kg^{-1}) was injected intravenously twice daily for five days in two 1.5-year-old and two 7–7.5-year-old monkeys. One 1.5-year-old monkey and the 7.5-year-old monkey were euthanized 10 weeks after BrdU injections; another 1.5-year-old monkey and the 7-year-old monkey were euthanized 15 weeks after BrdU injections. We analysed 52 sections for the presence of BrdU labelling in the brain of the 7.5-year-old macaque after a 10-week delay and 76 sections of the brain of the 7-year-old after a 15-week delay.

Immunohistochemistry. Frozen slides were allowed to equilibrate to room temperature for 3 h. Some antigens required antigen retrieval (Supplementary Table 3), which was conducted at 95 °C in 10 mM sodium citrate buffer, pH 6.0. Following antigen retrieval, slides were washed with TNT buffer (0.05% Triton-X100 in PBS) for 10 min, placed in 1% H_2O_2 in PBS for 45 min and then blocked with TNB solution (0.1 M Tris-HCl, pH 7.5, 0.15 M NaCl, 0.5% blocking reagent from PerkinElmer) for 1 h. Slides were incubated in primary antibodies overnight at 4 °C (Supplementary Table 3) and in biotinylated secondary antibodies (Jackson Immunoresearch Laboratories) for 2.5 h at room temperature. All antibodies were diluted in TNB solution. For most antibodies, the conditions of use were validated by the manufacturer (antibody product sheets). When this information was not provided, we performed control experiments, including no primary antibody (negative) controls and comparison to mouse staining patterns.

Sections were then incubated for 30 min in streptavidin–horseradish peroxidase, which was diluted (1:200) with TNB. Tyramide signal amplification (PerkinElmer) was used for some antigens. Sections were incubated in tyramide-conjugated fluorophores for 5 min at the following dilutions: fluorescein: 1:50; Cy3: 1:100; Cy5: 1:100. For sections that used the 3′,3′-diaminobenzidine (DAB) chromagenic immunohistochemistry method, the sections were first rinsed in PBS, incubated for 15 min in 1% H_2O_2, then incubated for 2 h in 10% fetal calf serum as the blocking buffer. This was followed by overnight incubation with the primary antibody at 4 °C, followed by incubation with the secondary antibody for 2 h at room temperature, and development using the VECTASTAIN ABC HRP system (Vector Laboratories). After several PBS rinses, sections were dehydrated, mounted and coverslipped. Staining was conducted in technical triplicates before analysis.

Fluorescent microscopy, image processing and quantifications. Images were acquired on Leica TCS SP8 or SP5 confocal microscopes using 10× (0.3 NA) or 63× (1.4 NA) objective lenses. Imaging of entire sections and for quantification of $DCX^+PSA\text{-}NCAM^+$ cells was carried out at 20× (0.45 NA) magnification on a Zeiss Axiovert 200M microscope or Keyence BZ-X Analyzer (BZX700) and individual files were stitched automatically. Imaging files were analysed and quantified in Neurolucida software (MBF Bioscience, 2017 version). Linear adjustments to image brightness and contrast were made equivalently across all images using Adobe Photoshop (CS 6). Cells were counted in *Z*-stack images from sections stained with Ki-67 and SOX2 or DCX and PSA-NCAM. Three to five representative images across a minimum of three evenly spaced and randomly sampled sections were collected for quantification at each age. Experimental replicates and different co-stains (in addition to the 3–5 sections included for quantifications) were also analysed for the presence or absence of young neurons or stem cells. The DG was subdivided into regions of interest (GCL, hilus or molecular layer) using DAPI to initially identify the cell-dense GCL. Each age has $n = 1$. Counts for cell populations were performed by three separate investigators who were blinded to individual cases. For each quantified marker, counts were repeated by different investigators for reproducibility. Fluorescence signal for single reactivity and co-localization of immunoreactivity was counted individually using the markers function in the Neurolucida imaging software. The quantification of data was performed with GraphPad Prism (v.6). No statistical methods were used to predetermine sample size.

Electron microscopy. For transmission electron microscopy (TEM), samples were sectioned with a vibrating blade microtome (200 μm) and post-fixed with 2% osmium tetroxide solution. Sections were dehydrated in increasing ethanol concentrations and stained with 2% uranyl acetate, embedded in araldite resin (Durcupan ACM Fluka, Sigma-Aldrich), and allowed to solidify at 69 °C for 72 h. We analysed 6 controls and 15 cases with epilepsy via TEM. We looked for the presence of cell clusters under light and electron microscopy in the 15 resected samples from patients with epilepsy that were 30–64 years old (at least 15 semi-thin sections per case) and 4 control samples from individuals that were 18–55 years old (45 semi-thin sections per case). In the additional control cases (samples from individuals that were 7 years old and 48 years old), we studied 100 semi-thin sections spanning the entirety of the anterior to posterior levels of the DG. Ultrathin sections were obtained (70 nm) for all controls and cases, and were contrasted with lead citrate solution on grids. Pre-embedding immunohistochemistry was performed on 50-μm floating sections with DCX and IBA1 antibodies. Post-fixation was performed with 7% glucose–1% osmium tetroxide, after which a conventional embedding protocol was followed. TEM micrographs of DCX immunolabelled ultrathin sections of the DG from individuals that were obtained at 22 gestational weeks of age (proximal edge), birth and 7 years of age were used for the GCL cellular profiles. All images were taken at the same magnification. Cell profiles were drawn on Adobe Photoshop by following the cytoplasmic cell membranes. Cells showing DCX immunogold labelling were coloured in red. DCX^- cells were identified by their ultrastructural characteristics: progenitors (light blue) had dark cytoplasm and few intermediate filaments and ensheathed DCX^+ cells; astrocytes (blue) had an irregular contour, star-shape morphology, light cytoplasm and intermediate filaments; mature neurons showed a large cell body with a large, round nucleus, and high amounts of ribosomes and organelles.

RNAscope *in situ* hybridization. Sequences of target probes, preamplifier, amplifier and label probes are proprietary and commercially available (Advanced Cell Diagnostics). Typically, the probes contain 20 ZZ probe pairs (approximately 50 bp per pair) covering around 1,000 bp. Here, we used a probe against human DCX targeting 181–1381 of NM_000555.3 as a single-plex probe. Slides for *in situ* hybridization were initially taken from −80 °C and dried at 60 °C for 1 h and fixed in 4% PFA for 2 h. After several PBS washes, slides were treated with ACD hydrogen peroxide for 10 min and then washed in water 2× before treatment in

1× target retrieval buffer (ACD) for 5 min (at 95–100 °C). After washing in water and then 100% alcohol, the slides were left to dry overnight before protease treatment for 15 min at 40 °C in the RNAscope oven. Hybridization of probes and amplification solutions was performed according the manufacturer's instructions. In brief, tissue sections were incubated in the desired probe (around 2–3 drops per section) for 2 h at 40 °C. The slides were washed twice in 1× wash buffer (ACD) for 2 min each. Amplification and detection steps were performed using the RNAscope 2.5 HD Red Detection Kit reagents (ACD, 320497) for single-plex probes. Sections were incubated with buffer Amp1 for 30 min at 40 °C and then washed twice in wash buffer for 2 min each. Amp2 was incubated on the sections for 15 min at 40 °C, followed by two washes in wash buffer. Sections were incubated in Amp3 for 30 min at 40 °C and washed twice in wash buffer for 2 min each, followed by incubation with Amp4 for 15 min at 40 °C. Slides were washed twice in wash buffer for 2 min each. Slides were incubated with Amp5 for 30 min at room temperature using the HybEZ humidity control tray and slide rack to maintain humidity. The slides were washed twice in 1× wash buffer for 2 min each and incubated in Amp6 for 15 min at room temperature before washing twice in wash buffer for 2 min each. The *in situ* hybridization signal was detected by diluting Fast RED-B in Fast RED-A solution (1:60 ratio) and incubating sections in this solution for 10 min. Slides were washed twice in water to stop the reaction.

Comparative gene transcription analysis. Developmental expression data were downloaded for human hippocampus (http://brainspan.org/; RPKM data; October 2013 release) and rhesus macaque hippocampus (http://blueprintnhpatlas.org/; March 2014 release). To compare laser-capture microdissected rhesus macaque samples to gross human hippocampus samples, we calculated average expression over all hippocampus samples for each age[33,34]. Expression data were *z*-score normalized for each species and ages were aligned between species based on calculated event scores of conserved timing of neurodevelopmental events[35].

Data availability. All data and/or analyses generated during the current study are available from the corresponding author upon reasonable request.

32. Mathern, G. W. *et al.* Seizures decrease postnatal neurogenesis and granule cell development in the human fascia dentata. *Epilepsia* **43,** 68–73 (2002).
33. Bakken, T. E. *et al.* A comprehensive transcriptional map of primate brain development. *Nature* **535,** 367–375 (2016).
34. Kang, H. J. *et al.* Spatio-temporal transcriptome of the human brain. *Nature* **478,** 483–489 (2011).
35. Workman, A. D., Charvet, C. J., Clancy, B., Darlington, R. B. & Finlay, B. L. Modeling transformations of neurodevelopmental sequences across mammalian species. *J. Neurosci.* **33,** 7368–7383 (2013).

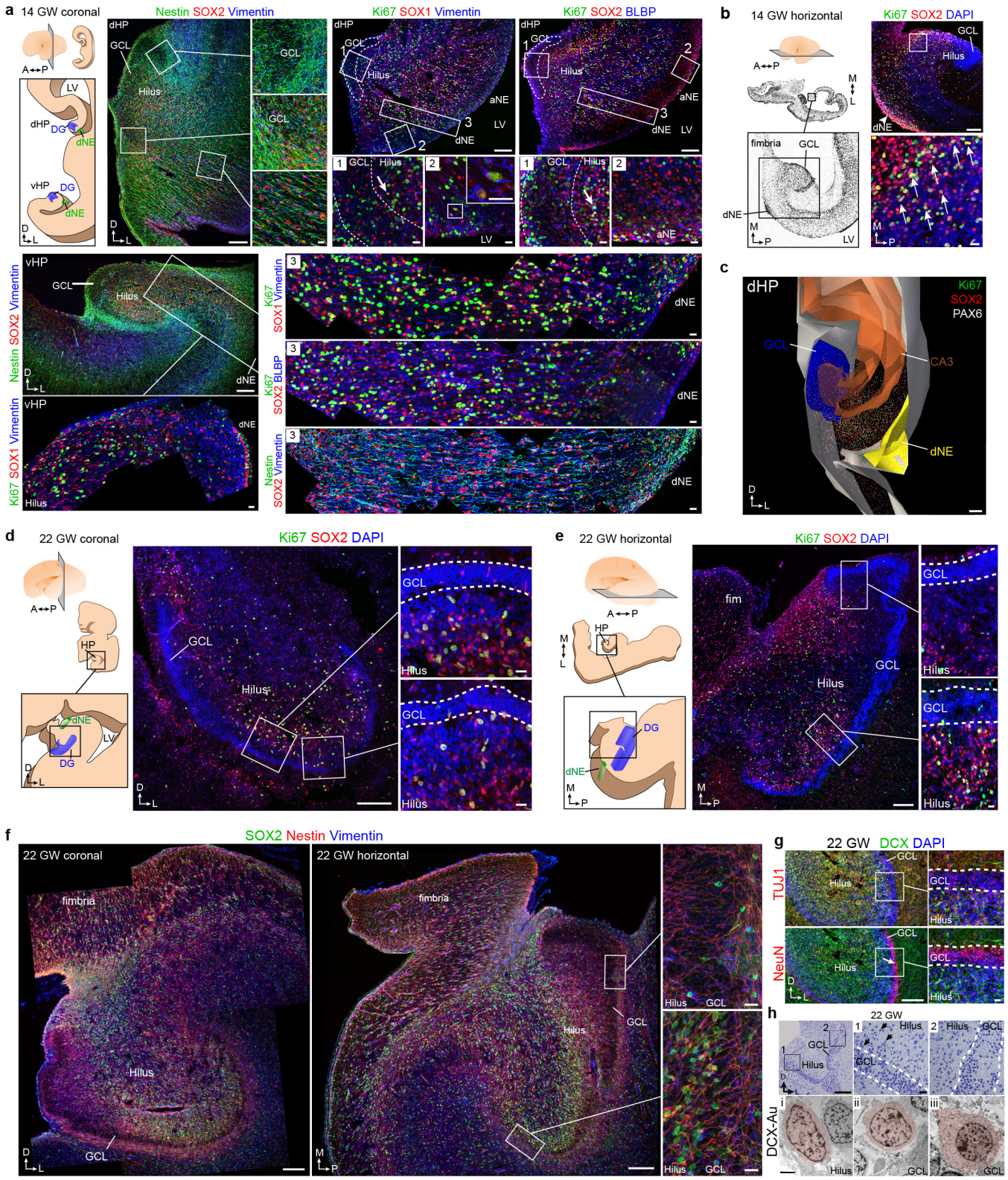

Extended Data Figure 1 | See next page for caption.

Extended Data Figure 1 | Additional marker and ultrastructural analysis of early fetal development of the human DG. a–c, Human brain of an individual at 14 gestational weeks. **a**, Schematic of the dorsal (dHP) and ventral (vHP) hippocampus in a coronal section. Precursor cells labelled with nestin, SOX2 and vimentin are organized in ribbons between the dNE and GCL. Ki-67$^+$ cells expressing SOX1 and vimentin or SOX2 and BLBP are present in the GCL and hilus (inset 1), along the wall of the lateral ventricle (LV) (inset 2) and between the GCL and the dNE (inset 3). The dNE is located at the edge of the ammonic neuroepithelium (aNE) closest to the fimbria. A similar organization is present in the vHP where nestin$^+$SOX2$^+$vimentin$^+$ cells connect the dNE to the developing GCL. Ki-67$^+$SOX1$^+$vimentin$^+$ cells are present in a strip along the ventricular wall and fill the region between the dNE and the GCL. **b**, Left, hemisphere at 14 gestational weeks, Nissl-stained horizontal sections. Right, Ki-67$^+$ cells expressing SOX2 (arrows). **c**, 3D reconstruction of the dHP showing the field of Ki-67$^+$ and SOX2$^+$ cells between the dNE and GCL. **d–h**, Human brain at 22 gestational weeks, coronal (**d**) and horizontal (**e**) sections. The hilus and GCL contain Ki-67$^+$SOX2$^+$ cells (**d**, **e** (insets)) as well as nestin$^+$SOX2$^+$vimentin$^+$ cells (**f**). These populations are asymmetrically distributed; sparse in the medial (proximal) GCL and hilus (top insets in **e**, **f**) but abundant in the lateral (distal) GCL and hilus (bottom insets in **e**, **f**). **g**, DCX$^+$TUJ1$^+$ cells and NeuN$^+$ cells in the DG at 22 gestational weeks. NeuN$^+$ GCL neurons in the distal GCL (arrow). **h**, A toluidine-blue-stained semi-thin section (top) and TEM micrographs showing the ultrastructural characteristics of DCX immunogold-labelled cells (pseudocoloured, bottom) at 22 gestational weeks. Insets of the semi-thin section show the proximal (1) and distal (2) ends of the GCL. Most DCX$^+$ cells in the hilus and the proximal GCL have little cytoplasm, few organelles and a small, irregular nucleus (i, ii); some DCX$^+$ cells in the hilus have an elongated, fusiform morphology (i). Some DCX$^+$ cells in the GCL have mature neuronal characteristics such as a round nucleus, more cytoplasm, ribosomes, rough endoplasmic reticulum and mitochondria (iii); this cell type was more common in the distal GCL. At this stage, the round and more mature neuronal morphologies were observed in the distal, but not in the proximal, blade. Scale bars, 200 μm (**a–h** (left images)), 2 μm (**a–h** (insets)) and 2 μm (**h** (TEM)).

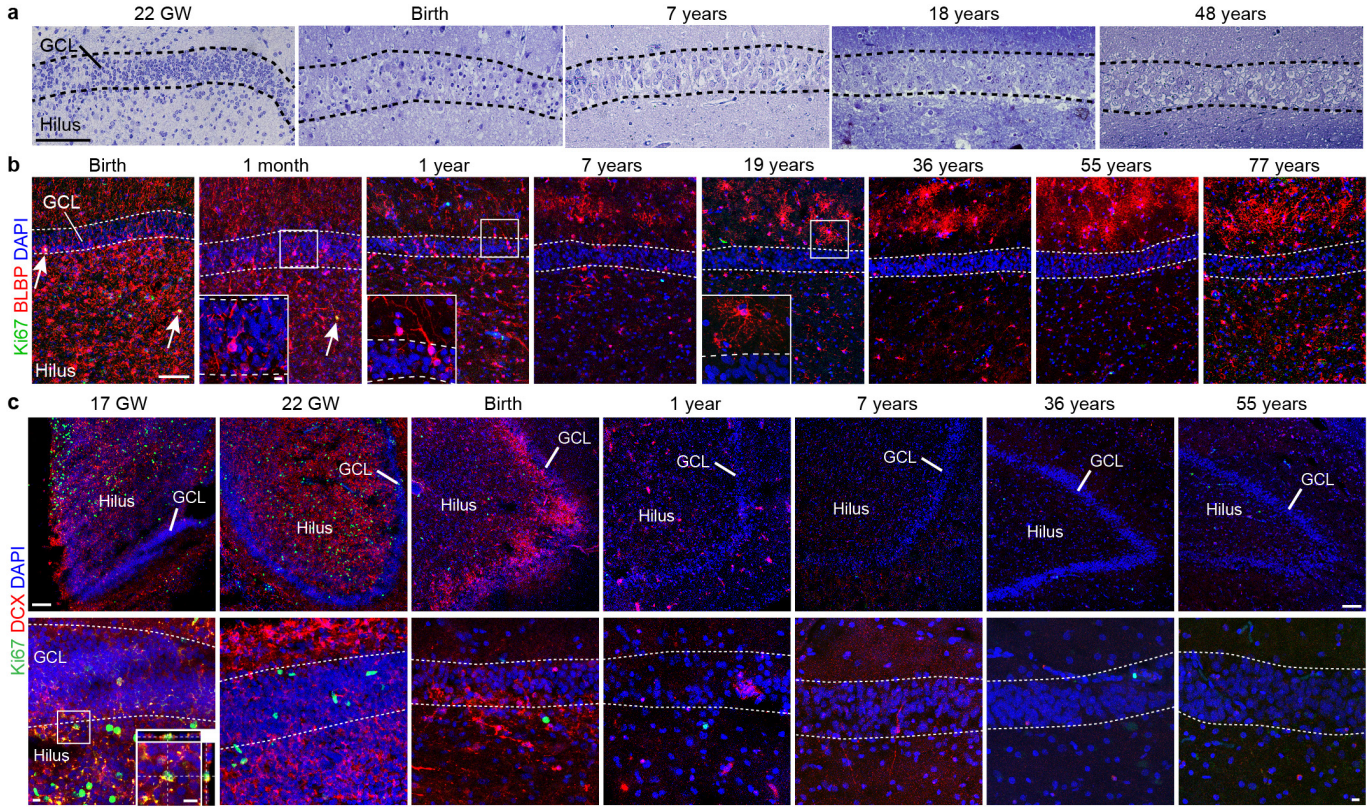

Extended Data Figure 2 | A coalesced proliferative SGZ does not form in the human DG; additional marker expression. a, Toluidine-blue-counterstained semi-thin sections of the human GCL from fetal to adult ages. Note that a discrete cellular layer does not form next to the GCL and the small dark cells characteristic of SGZ precursors are not present (compare to Extended Data Fig. 9b in the macaque). **b**, $BLBP^+$ cells are distributed broadly in the DG from birth to 1 year, many of these cells have a radial morphology (see insets) and some co-express Ki-67 at birth and 1 month (double-positive cells are indicated by the arrows). By 7 years and in adults, most BLBP is present in the molecular layer in stellate protoplasmic astrocytes. **c**, $DCX^+Ki\text{-}67^+$ cells in the GCL are rare at 17 gestational weeks (orthogonal views, inset) but were abundant in the ganglionic eminence at the same age (data not shown). $DCX^+Ki\text{-}67^+$ cells were absent in the GCL from 22 gestational weeks to 55 years. Scale bars, 100 μm (**a–c**) and 10 μm (**a–c** (insets)).

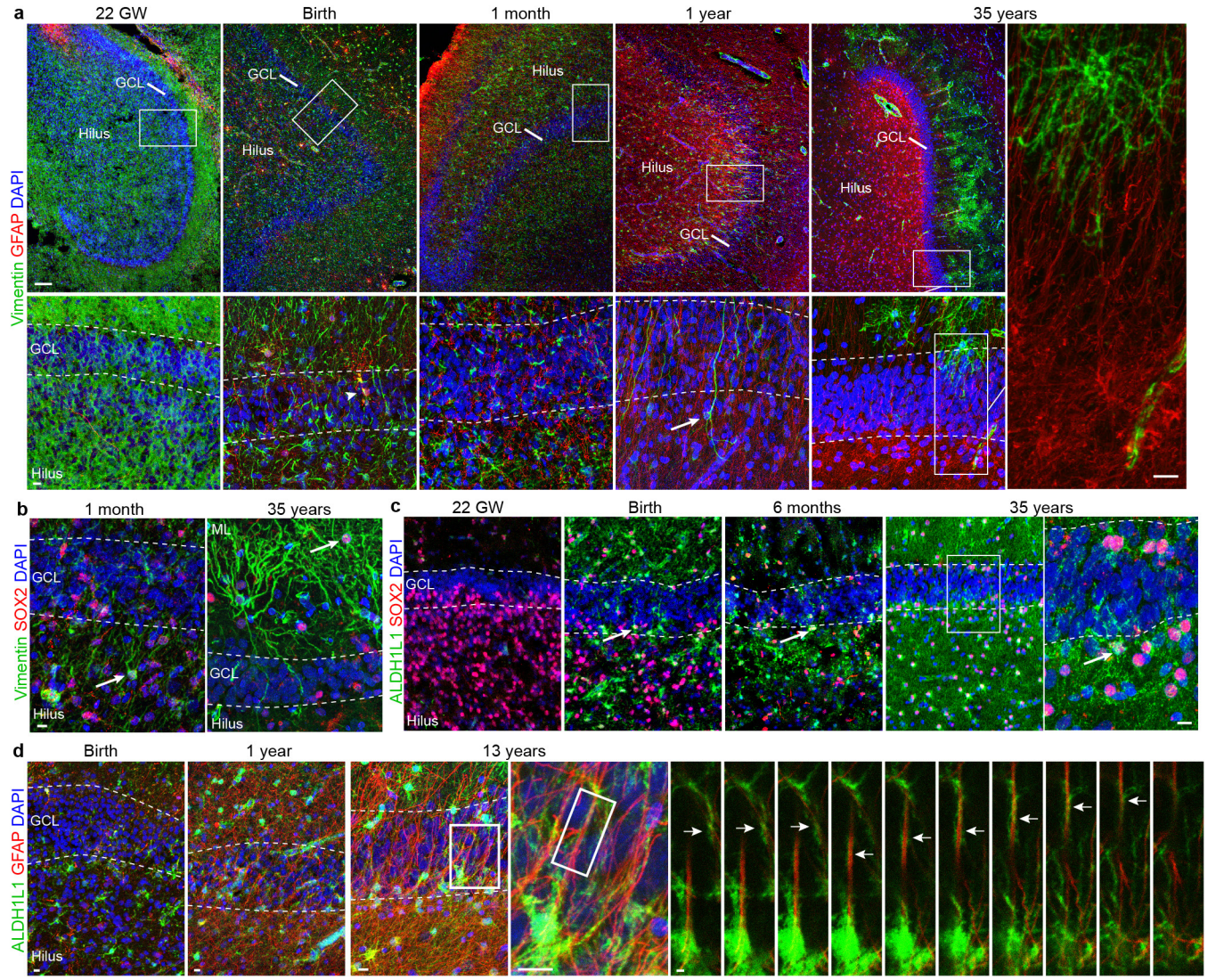

Extended Data Figure 3 | Additional marker expression for astroglial cells and progenitor cells in the human DG at different ages. **a**, Vimentin$^+$ and GFAP$^+$ cells in the hippocampus from 22 gestational weeks to 35 years. Vimentin is widely expressed during fetal and early postnatal development and is mostly restricted to protoplasmic astrocytes in the molecular layer in adults. GFAP is not expressed at 22 gestational weeks, but at birth a few vimentin$^+$GFAP$^+$ cells are present in the hilus and GCL (arrowhead). Interestingly, some vimentin$^+$GFAP$^-$ cells with a radial morphology (arrow) are observed in samples at 1 year of age, but not at the other ages. In adults, GFAP and vimentin are not co-expressed (right, high-magnification of thin GFAP$^+$vimentin$^-$ fibres within the GCL). **b**, Vimentin$^+$Sox2$^+$ simpler elongated cells in the hilus at 1 month (arrow) and protoplasmic astrocytes in the molecular layer at 35 years of age (arrow). **c**, SOX2$^+$ cells are abundant in the GCL and hilus at 22 gestational weeks, and co-express ALDH1L1 in the brain at birth and in older individuals (arrows). **d**, At birth, there are few ALDH1L1$^+$GFAP$^+$ cells in the DG, but by 13 years of age many stellate astrocytes express both of these markers. Right, *z* stack of radial GFAP$^+$ processes that are surrounded by ALDH1L1 staining. Scale bars, 100 μm (**a** (top row)), 10 μm (**a** (bottom row and insets), **b**–**d**) and 2 μm (**d** (*z*-stack)).

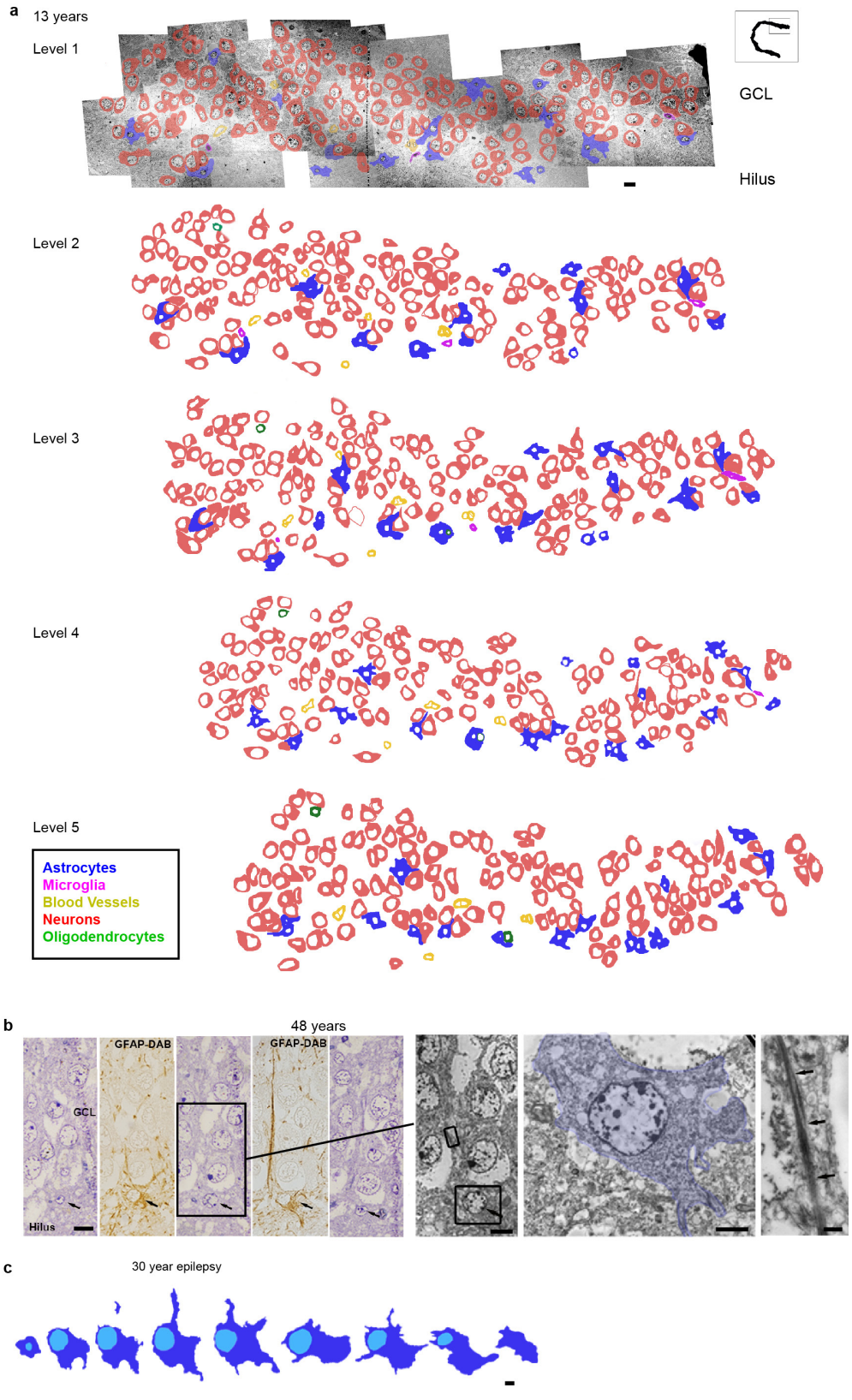

Extended Data Figure 4 | See next page for caption.

Extended Data Figure 4 | TEM analysis of cell types in the DG of human brains obtained from a 13-year-old individual and an adult; absence of SGZ precursor cells or immature neurons. a, Reconstruction of 5 ultrathin sections (separated by 1.5 μm) from the GCL of the 13-year-old individual with outlines of cell membranes. Colours corresponding to the different cell types defined by their ultrastructural characteristics are indicated in the key. No clusters or isolated cells with a young neuronal ultrastructure were found. Cells associated in small groups were identified as astrocytes, oligodendrocytes or microglia. **b**, **c**, Reconstructions of astroglial cells next to the GCL, searching for possible examples of radial astrocytes in the DG of an adult human. **b**, Example of an astrocyte with radial morphology in the adult GCL. Five serial semi-thin sections of this astrocyte (black arrows) next to the GCL of the DG of a 48-year-old individual are shown; alternating semi-thin sections show that this cell is $GFAP^+$. This cell extends a thin radial fibre through the GCL, but has multiple processes (stellate morphology) in the hilus. Boxed area shows the ultrastructure from the indicated semi-thin section of this astrocyte (pseudocoloured in blue) and the bundles of intermediate filaments present in the expansion (arrows). **c**, Another example of a serially reconstructed astrocyte in the DG of a 30-year-old individual with epilepsy (separated by 1.4 μm), showing a short radial expansion and processes into the hilus. Scale bars, 10 μm (**a**, **b**, semi-thin sections and TEM micrographs), 5 μm (**c**), 2 μm (**b**, soma) and 500 nm (**b**, intermediate filaments).

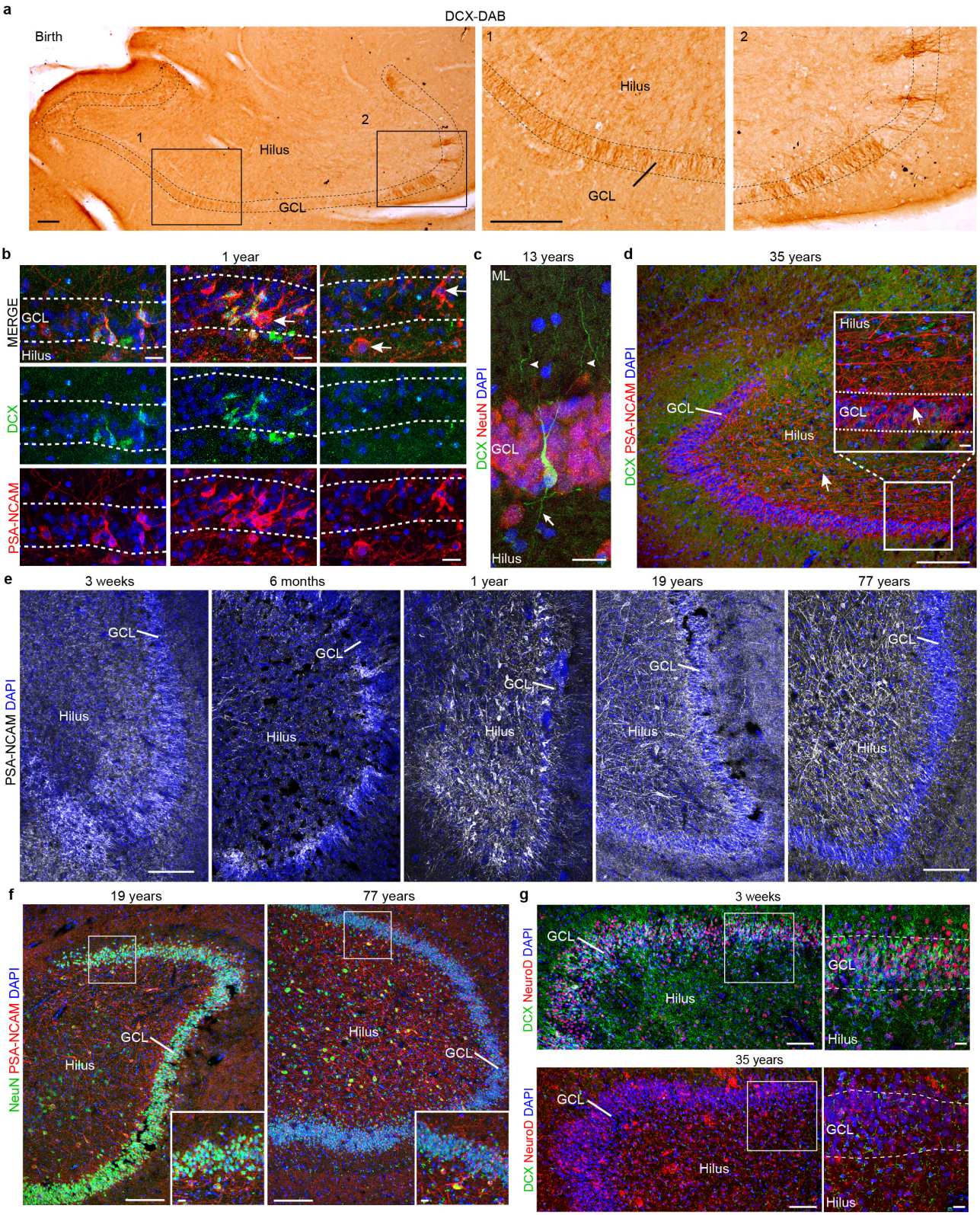

Extended Data Figure 5 | Young neurons are present in the infant but not the adult human DG. a, DAB staining in the hippocampus at birth reveals many young neurons in the GCL. **b**, $DCX^+PSA\text{-}NCAM^+$ cells are distributed in clusters across the GCL at 1 year of age. Most $PSA\text{-}NCAM^+$ cells are DCX^+, but some are $DCX^-PSA\text{-}NCAM^+$ (arrows). **c**, In the samples from a 13-year-old individual, DCX^+ cells have a more mature neuronal morphology. The cell shown is $NeuN^+$ and has dendrites in the molecular layer (arrowheads) and an axon projecting into the hilus (arrow). **d**, At 35 years of age, the DG does not contain $DCX^+PSA\text{-}NCAM^+$ cells, but does contain many $DCX^-PSA\text{-}NCAM^+$ cells that do not have the morphology of young neurons. **e**, $PSA\text{-}NCAM^+$ staining in the human DG from 3 weeks to 77 years; in adults, these cells have a more mature neuronal morphology and are localized in the hilus. **f**, $PSA\text{-}NCAM^+$ cells in the DG are $NeuN^+$ in samples of 19- and 77-year-old individuals. **g**, At 3 weeks of age, the GCL and hilus were filled with clusters of $DCX^+NeuroD^+$ cells, and many of the DCX^- GCL neurons were $NeuroD^+$. At 35 years, no $DCX^+NeuroD^+$ cells were observed; antibody labelling for NeuroD was non-specific. Scale bars, 200 μm (**a**, **d**–**g**), 20 μm (**b**, **c**, and **d**, **f**, **g** (inset)).

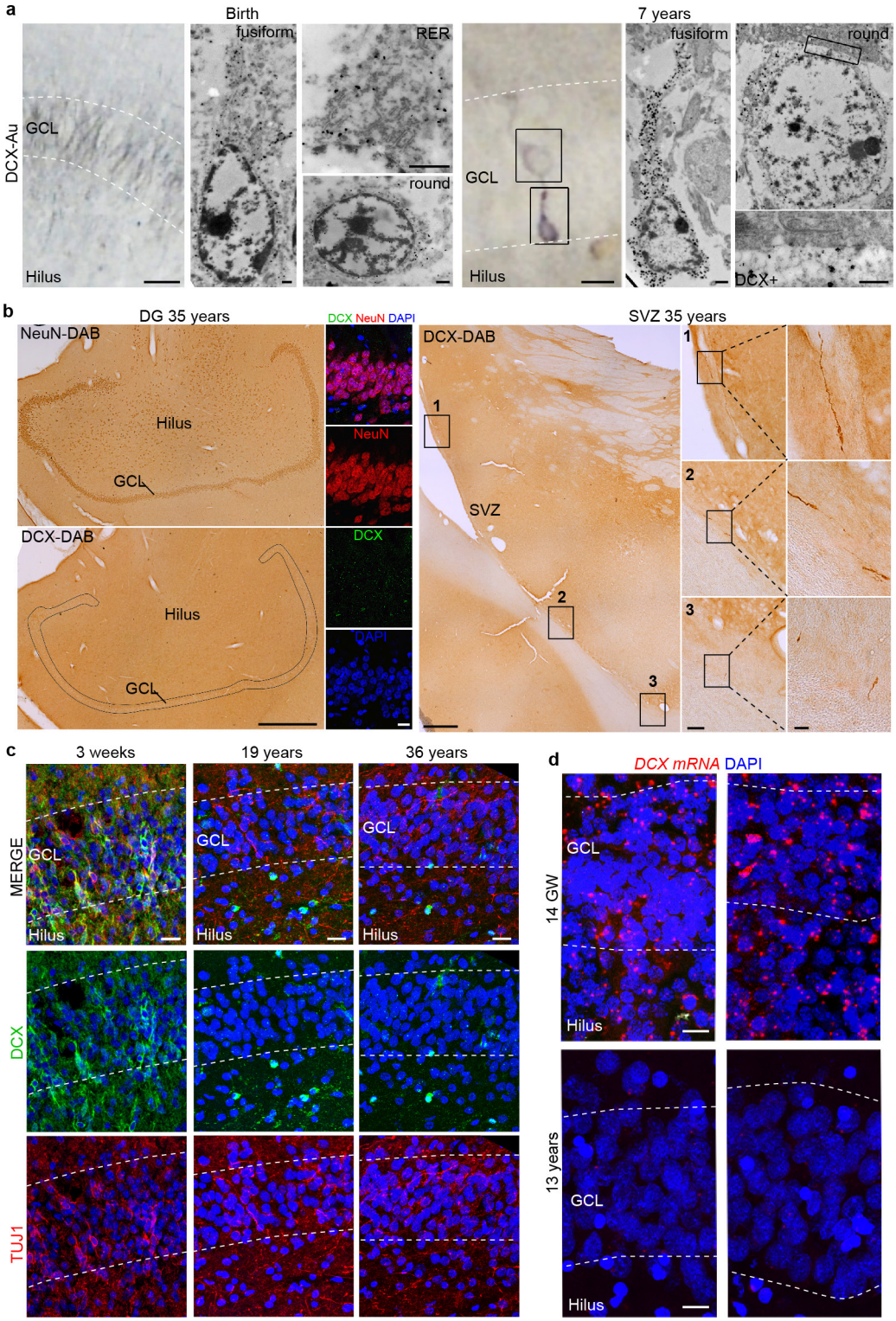

Extended Data Figure 6 | DCX$^+$ young neurons in the developing human hippocampus. a, TEM micrographs of DCX immunogold staining at birth and 7 years of age. At birth, the GCL contains small DCX$^+$ cells with little cytoplasm, rough endoplasmic reticulum (RER) cisternae and a fusiform or round nucleus. At 7 years of age, DCX$^+$ cells closer to the hilus have characteristics of immature neurons, including few organelles and a long expansion towards the GCL. DCX$^+$ cells located within the GCL have mature neuron characteristics, including a large, round nucleus, rough endoplasmic reticulum, mitochondria and microtubules consistent with a more mature neuronal morphology (see Extended Data Fig. 5). At higher magnification, the more mature-appearing DCX-labelled cells are adjacent to DCX$^-$ GCL neurons. **b**, No DCX$^+$ cells in the hilus and GCL (stained by NeuN antibodies; left insets) were found in the brain of a 35-year-old individual that showed exceptional preservation. In this sample, rare DCX$^+$ cells with the features of young migratory neurons were present in the ventricular–subventricular zone (right insets). SVZ, subventricular zone. **c**, DCX$^+$TUJ1$^+$ cells were present in the GCL and hilus at 3 weeks of age, but were not detected in the adult DG. **d**, RNA-scope detection of *DCX* mRNA revealed many cells in the DG at 14 gestational weeks, but weakly labelled cells distributed throughout in the DG and other regions of the hippocampus at 13 years of age. Scale bars: 1 mm (**b** (left)), 100 μm (**b** (middle right inset)), 20 μm (**b** (right insets), **c**), 10 μm (**d**), 5 μm (**a** (left)) and 500 nm (**a** (right, TEM)).

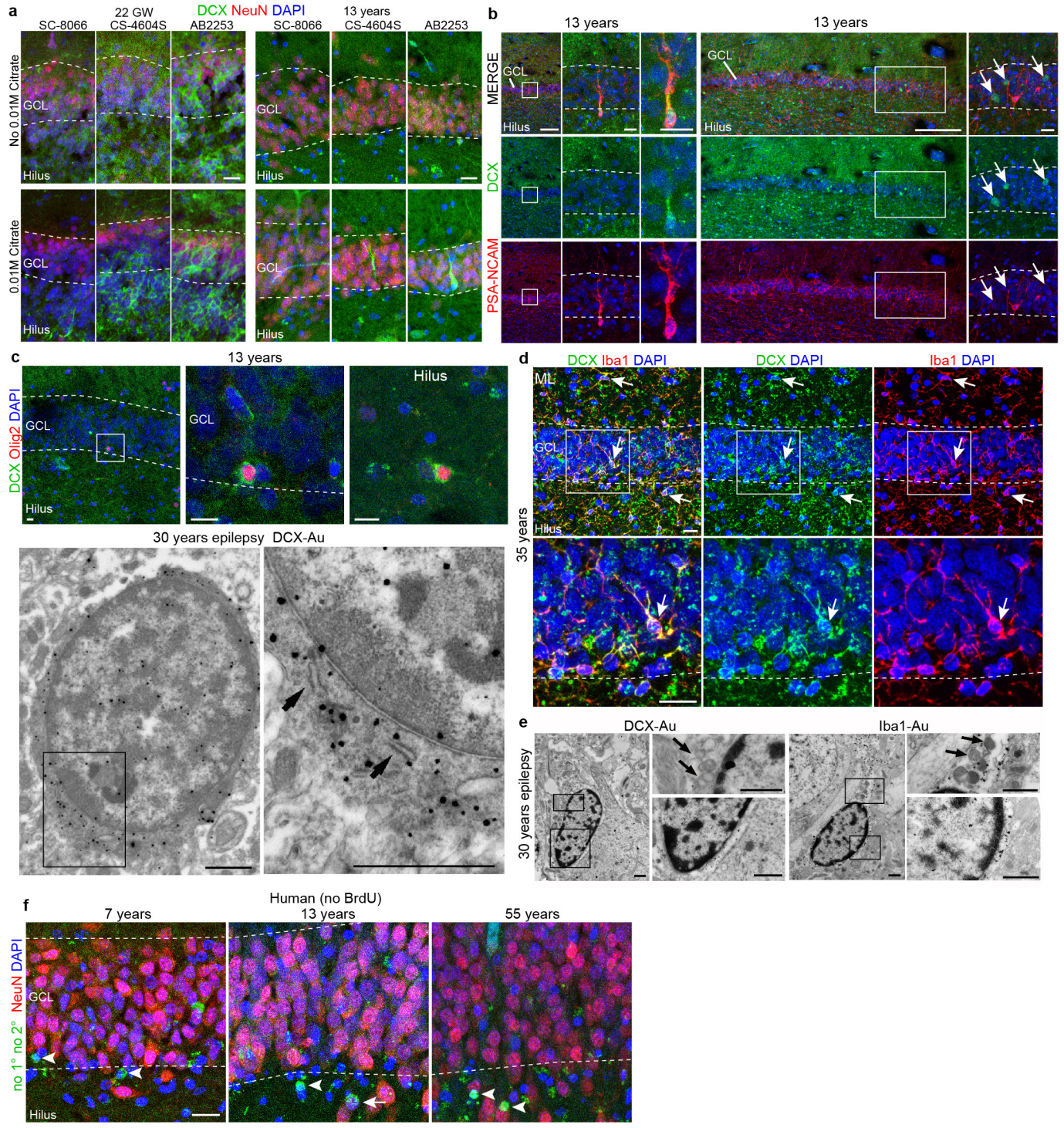

Extended Data Figure 7 | DCX$^+$PSA-NCAM$^-$ glial cells in the adult human hippocampus. a, Comparison of citrate antigen retrieval using three DCX antibodies from this study (SC-8066, CS-4604S and AB2253) in the GCL obtained from individuals at 22 gestational weeks and 13 years of age. The 13 year old DCX$^+$ cell (Extended Data Fig. 5c) is shown in the lower right panel and adjacent sections were stained with the other antibodies. **b**, Example of a DCX$^+$PSA-NCAM$^+$ neuron in the GCL and DCX$^+$PSA-NCAM$^-$ staining in the sample from the 13-year-old individual (arrows). **c**, Examples of DCX$^+$OLIG2$^+$ cells in the GCL and hilus of the 13-year-old individual. Immunogold-labelled DCX$^+$ cells viewed by TEM had single short endoplasmic reticulum cisternae (arrows), a very irregular contoured membrane and a round nucleus with condensed chromatin characteristic of oligodendrocytes. **d**, In some samples (see Extended Data Fig. 5g, bottom right inset), we found DCX$^+$ immunoreactivity in many small multipolar cells. This staining was not limited to the hilus, or GCL, but was present in cells across the tissue and co-localized with the microglial marker IBA1 (arrows). **e**, TEM micrographs of DCX and IBA1 immunogold-labelled cells in an adult DG of a 30-year-old individual with epilepsy. DCX$^+$ and IBA1$^+$ cells have similar characteristics: elongated nucleus with clumps of chromatin beneath the nuclear envelope and throughout the nucleoplasm, irregular contour and the presence of lysosomes and lipofucsin (arrows). Note that these features are typical of microglial cells. **f**, Human hippocampus stained with NeuN followed by processing for BrdU detection (with no primary or secondary antibodies) shows round fluorescent signal (arrowheads indicate signal that is NeuN$^-$) occasionally overlapping with NeuN staining (arrow). Scale bars, 200 μm (**b** (left column and wide column)), 20 μm (**a**, **b** (left-middle columns, right column), **d**, **f**), 10 μm (**c** (top row)) and 1 μm (**c** (bottom row), **e**).

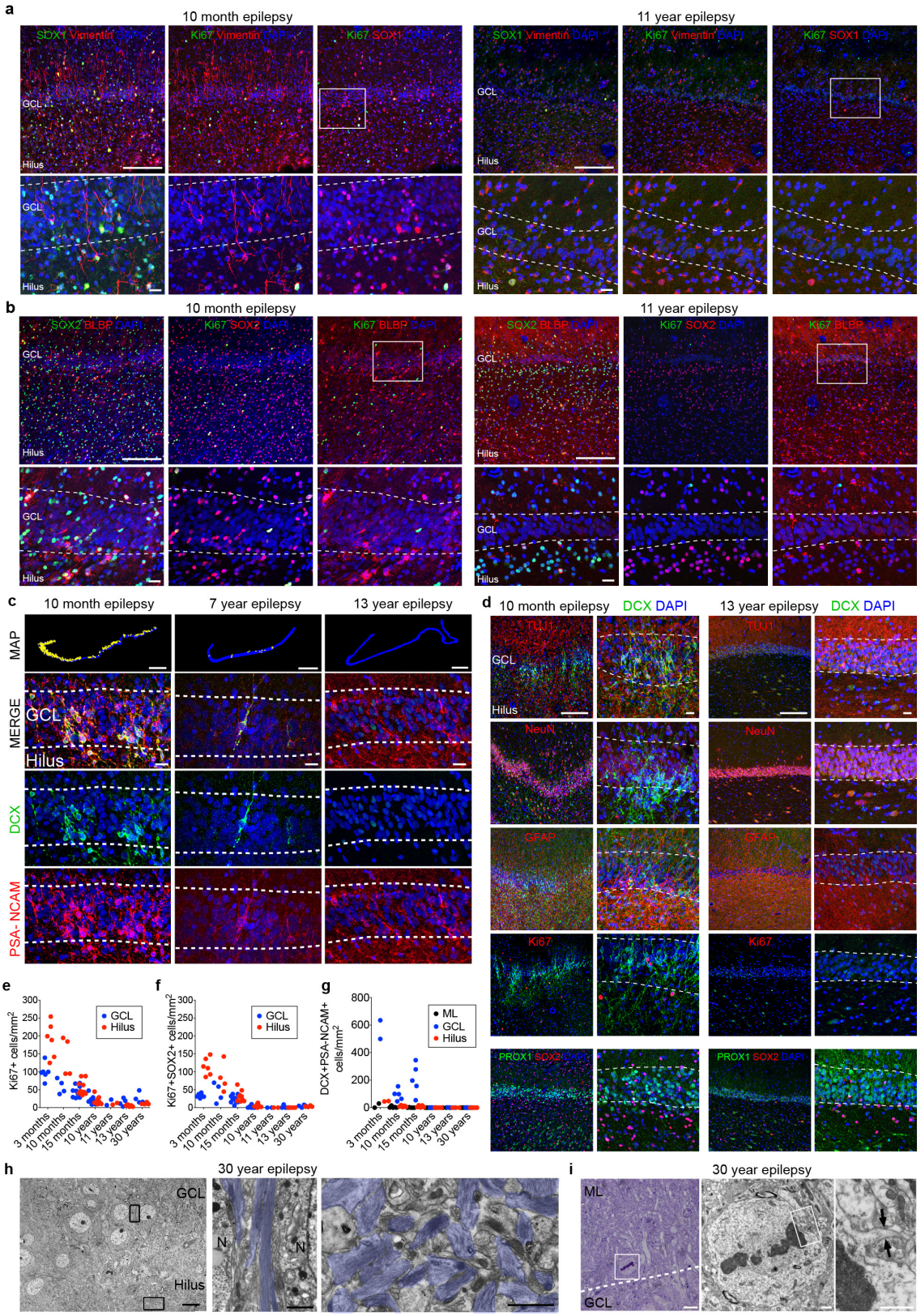

Extended Data Figure 8 | See next page for caption.

Extended Data Figure 8 | Neurogenesis declines in patients with epilepsy from infancy into childhood. **a**, Ki-67$^+$SOX1$^+$vimentin$^+$ cells are located in the hilus and GCL at 10 months but are not present at 11 years of age. **b**, Ki-67$^+$SOX2$^+$BLBP$^+$ cells are located in the hilus and GCL at 10 months but are not present at 11 years of age. **c**, Maps of DCX$^+$PSA-NCAM$^+$ cells (yellow dots) and representative immunostaining at 10 months, 7 years and 13 years (bottom rows). **d**, In the 10-month-old DG of a patient with epilepsy, DCX$^+$ cells co-expressing PSA-NCAM or TUJ1 are distributed throughout the NeuN$^+$PROX1$^+$ GCL, but do not co-express Ki-67 or GFAP. In the DG of a 13-year-old patient with epilepsy, DCX$^+$ cells co-expressing PSA-NCAM or TUJ1 were not present. Few Ki-67$^+$ cells were visible throughout the DG. **e–g**, Quantification of Ki-67$^+$ (**e**), Ki-67$^+$SOX2$^+$ (**f**) and DCX$^+$PSA-NCAM$^+$ (**g**) cells in the DG of surgically resected hippocampuses. **h**, TEM micrographs of the brain of a 30-year-old patient with epilepsy showing astroglial expansions with high number of intermediate filaments (blue) ensheathing GCL neuronal bodies. A dense network of astrocytic expansions in the hilus, containing dense bundles of intermediate filaments (blue), fills the region proximal to the GCL with no evidence of SGZ progenitor cells. **i**, Mitotic cells are very rare and not restricted to the hilus or GCL. A toluidine-blue-stained 1.5-μm section from the DG of a 30-year-old brain shows a dividing cell in the molecular layer, adjacent to the GCL. The TEM micrograph shows the dividing cell in metaphase with a light cytoplasm, few organelles and an irregular contour with a small expansion (arrows), which are characteristic of astrocytes (shown at higher magnification). N, neuron. For quantifications, staining replicates ($\geq$3) are shown by dots (each age, $n = 1$). Scale bars, 1 mm (**c** (maps)), 200 μm (**a**, **b** (top), **d** (left)), 20 μm (**a–c** (bottom), **d** (right)) and 10 μm (**h**, **i** (left)), 1 μm (**h**, **i** (middle and right)).

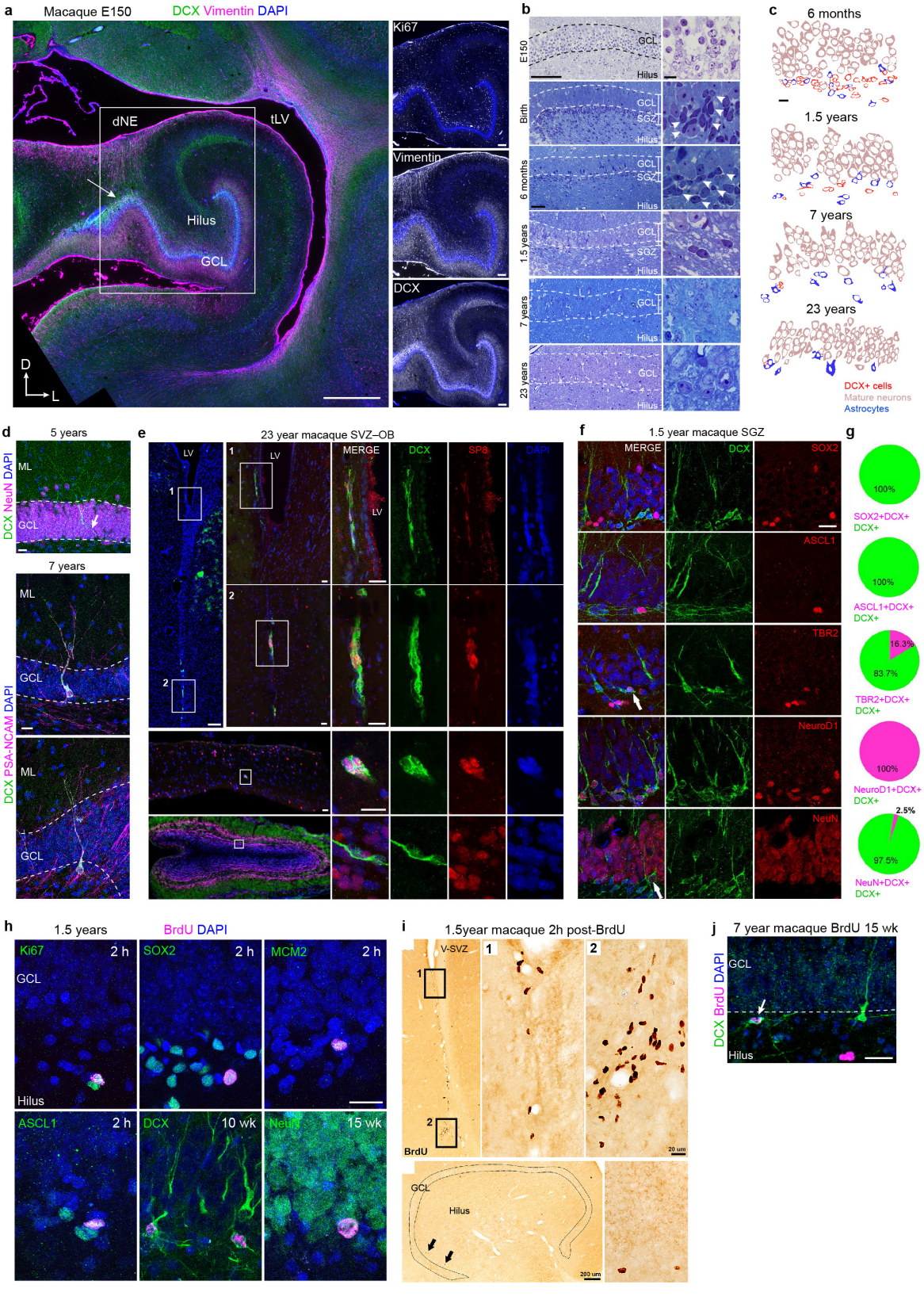

Extended Data Figure 9 | See next page for caption.

Extended Data Figure 9 | Development of the macaque DG and evidence of the presence of a proliferative SGZ and postnatal neurogenesis with a sharp decline in adulthood. a, The E150 macaque hippocampus has many Ki-67$^+$ cells in the SGZ as well as vimentin$^+$ fibres and DCX$^+$ cells between the dNE and the GCL (arrow). **b**, Toluidine-blue-stained semi-thin sections of the macaque DG reveal small and dark condensed nuclei (arrows) in the SGZ from fetal ages (E150) to 1.5 years; few are visible in the DG at 7 years of age and these cells are very rare in the DG of a 23-year-old macaque (compare with human data in Extended Data Fig. 2a). **c**, Profiles of the cellular populations in the macaque DG at 6 months, 1.5, 7 and 23 years of age. As in the human DG, DCX$^+$ cells decrease markedly with age and have little cytoplasm and a smaller nucleus compared to mature granule neurons. **d**, Top, example of a DCX$^+$NeuN$^+$ cell with mature dendrites in the GCL of a 5-year-old macaque. Middle, bottom, two examples of DCX$^+$PSA-NCAM$^+$ cells with dendritic arborization present in the GCL of a 7.5-year-old macaque. An axonal extension (arrow) into the hilus is visible. **e**, The ventricular–subventricular zone (SVZ) and olfactory bulb (OB) of a 23-year-old macaque contain some DCX$^+$SP8$^+$ cells with the morphology of young neurons, but similar cells are rare in the GCL of the 23-year-old macaque (Fig. 4b, d). **f**, DCX$^+$ cells in the SGZ of a 1.5-year-old macaque express transcription factors in common with those in the mouse SGZ. **g**, Percentages of DCX$^+$ cells expressing markers shown in **f**. **h**, Immunostaining images of BrdU$^+$ cells and cell proliferation (Ki-67, MCM2), progenitor cell markers (SOX2, ASCL1) or DCX, in the 1.5-year-old macaque euthanized 2 h after BrdU injection. BrdU$^+$DCX$^+$ and BrdU$^+$NeuN$^+$ cells could be identified 10 or 15 weeks after BrdU exposure, respectively. **i**, DAB-staining for BrdU in the ventricular–subventricular zone and SGZ of a 1.5-year-old macaque, 2 h after BrdU injection. **j**, Example of a rare DCX$^+$BrdU$^+$ cell in the 7.5-year-old macaque. Scale bars, 1 mm (**a** (left)) 200 μm (**a** (right), **e** (top left, bottom left), **i** (left)), 100 μm (**b** (left)), 20 μm (**d**, **e** (middle left and right), **f**, **h**, **i** (right), **j**) and 10 μm (**b** (right), **c**).

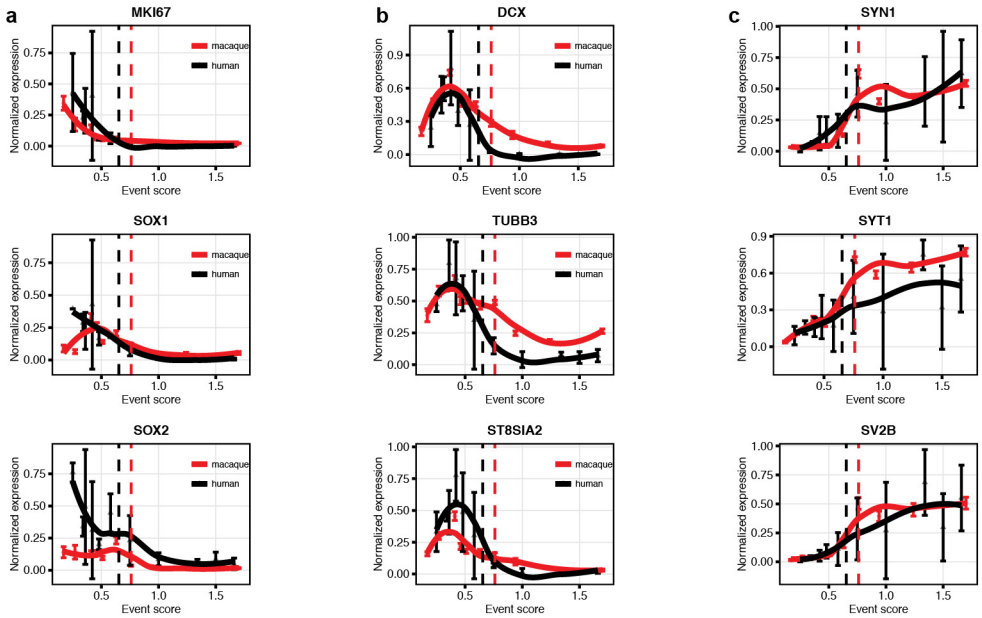

Extended Data Figure 10 | Decline in markers associated with neurogenesis in the macaque and human hippocampus (gene-expression profiling). a, Markers of dividing or precursor cells. **b**, Markers of young neurons. **c**, Markers of mature neurons. Human RNA-seq (http://brainspan.org/) and macaque expression profiling (dataset from ref. 33) developmental data from hippocampus for the indicated genes. Human data are averaged over biological replicates by developmental period (as defined in ref. 34). Normalized data are plotted on the same developmental event scale. Loess-fit curves are displayed with data points (mean ± s.e.m.). Dashed lines indicate birth.

nature research

Corresponding author(s): Arturo Alvarez-Buylla, Zhengang Fang, Jose Manuel Verdugo

Life Sciences Reporting Summary

Nature Research wishes to improve the reproducibility of the work that we publish. This form is intended for publication with all accepted life science papers and provides structure for consistency and transparency in reporting. Every life science submission will use this form; some list items might not apply to an individual manuscript, but all fields must be completed for clarity.

For further information on the points included in this form, see Reporting Life Sciences Research. For further information on Nature Research policies, including our data availability policy, see Authors & Referees and the Editorial Policy Checklist.

Please do not complete any field with "not applicable" or n/a. Refer to the help text for what text to use if an item is not relevant to your study.

For final submission: please carefully check your responses for accuracy; you will not be able to make changes later.

Experimental design

1. Sample size

Describe how sample size was determined.

Sample size was not predicted. This was not needed as there were no statistical comparisons performed.

2. Data exclusions

Describe any data exclusions.

No data was excluded.

3. Replication

Describe the measures taken to verify the reproducibility of the experimental findings.

Experiments were repeated at minimum in triplicates.

4. Randomization

Describe how samples/organisms/participants were allocated into experimental groups.

Randomization was not relevant as no statistical analyses or comparisons were performed.

5. Blinding

Describe whether the investigators were blinded to group allocation during data collection and/or analysis.

Investigators who performed quantifications were blinded on individual cases that were being analyzed. This is described in the Materials and Methods section, under "Fluorescent microscopy, image processing, and quantifications".

Note: all in vivo studies must report how sample size was determined and whether blinding and randomization were used.

6. Statistical parameters

For all figures and tables that use statistical methods, confirm that the following items are present in relevant figure legends (or in the Methods section if additional space is needed).

n/a	Confirmed
☐	☒ The exact sample size (*n*) for each experimental group/condition, given as a discrete number and unit of measurement (animals, litters, cultures, etc.)
☐	☒ A description of how samples were collected, noting whether measurements were taken from distinct samples or whether the same sample was measured repeatedly
☐	☒ A statement indicating how many times each experiment was replicated
☒	☐ The statistical test(s) used and whether they are one- or two-sided *Only common tests should be described solely by name; describe more complex techniques in the Methods section.*
☒	☐ A description of any assumptions or corrections, such as an adjustment for multiple comparisons
☒	☐ Test values indicating whether an effect is present *Provide confidence intervals or give results of significance tests (e.g. P values) as exact values whenever appropriate and with effect sizes noted.*
☒	☐ A clear description of statistics including central tendency (e.g. median, mean) and variation (e.g. standard deviation, interquartile range)
☒	☐ Clearly defined error bars in all relevant figure captions (with explicit mention of central tendency and variation)

See the web collection on statistics for biologists for further resources and guidance.

Software

Policy information about availability of computer code

7. Software

Describe the software used to analyze the data in this study.	Commercially available software, MBF Neurolucida, Graphpad Prism, and Adobe Creative Suite, and ImageJ were used. This is mentioned in relevant sections in the Materials and Methods section, with software versions annotated.

For manuscripts utilizing custom algorithms or software that are central to the paper but not yet described in the published literature, software must be made available to editors and reviewers upon request. We strongly encourage code deposition in a community repository (e.g. GitHub). *Nature Methods* guidance for providing algorithms and software for publication provides further information on this topic.

Materials and reagents

Policy information about availability of materials

8. Materials availability

Indicate whether there are restrictions on availability of unique materials or if these materials are only available for distribution by a third party.	There are no restrictions to availability of human and macaque tissue used. Tissue was collected under institutional guidelines. This is described in the Materials and Methods section, under "Human Tissue Collection".

9. Antibodies

Describe the antibodies used and how they were validated for use in the system under study (i.e. assay and species).	We generated a table (Supplementary Table 3) which lists every antibody used in the manuscript, the catalog number, and conditions of utilization. We have also added information re species validation, which is now included as product notes in Supplementary table 3. For most antibodies, species was validated by company and indicated (information taken from antibody product sheets). When this was not provided, we performed control experiments, including no primary antibody (negative) controls and comparison to mouse staining patterns.

10. Eukaryotic cell lines

a. State the source of each eukaryotic cell line used.	No eukaryotic cell lines were used.
b. Describe the method of cell line authentication used.	No eukaryotic cell lines were used.
c. Report whether the cell lines were tested for mycoplasma contamination.	No eukaryotic cell lines were used.
d. If any of the cell lines used are listed in the database of commonly misidentified cell lines maintained by ICLAC, provide a scientific rationale for their use.	No eukaryotic cell lines were used.

Animals and human research participants

Policy information about studies involving animals; when reporting animal research, follow the ARRIVE guidelines

11. Description of research animals

Provide all relevant details on animals and/or animal-derived materials used in the study.	Animal material used in this study came from certified and regulated breeding colonies at Fudan University and the University of California, Davis. Details are described in Materials and Methods section under "Macaque Tissue Preparation" and in Supplementary Table 2. As

Policy information about studies involving human research participants

12. Description of human research participants

Describe the covariate-relevant population characteristics of the human research participants.	For controls, tissue had normal pathological diagnosis. For epilepsy cases, all tissue was from intractable seizure cases. This is described in the Materials and Methods section, under "Human Tissue Collection" as well as Supplementary Table 1. This section also contains the information regarding how informed consent was obtained for tissue acquisition.